Soil Dynamics and Earthquake Engineering 106 (2018) 70–89

Contents lists available at ScienceDirect

Soil Dynamics and Earthquake Engineering

journal homepage: www.elsevier.com/locate/soildyn

Empirical scaling relations for pseudo relative velocity spectra in western Himalaya and northeastern India

I.D. Gupta[a], M.D. Trifunac[b,*]

[a] Independent Scholar, Row House 4, Suncity, Pune 411051, India
[b] Dept. of Civil Engineering, Univ. of Southern California, Los Angeles, CA 90089, United States

ARTICLE INFO

Keywords:
Strong-motion attenuation models
Pseudo relative velocity spectrum
Western Himalaya
Northeastern India
Regression analysis
Seismic hazard

ABSTRACT

In this paper, frequency-dependent empirical scaling equations are developed for pseudo relative velocity (*PSV*) spectrum amplitudes of strong earthquake ground accelerations in western Himalaya and northeastern India for five ratios of critical damping $\zeta = 0.00, 0.02, 0.05, 0.10$, and 0.20. These are based on the frequency-dependent attenuation functions developed in our recent work (Gupta and Trifunac [38]) for these two regions. The proposed scaling relations are shown to have physically realistic dependence on earthquake magnitude, source-to-site distance, and local site geological and soil conditions. The extension of the empirical *PSV* amplitudes to short and long periods, beyond the empirical period range, is also illustrated using available techniques (Trifunac [89,90]). To demonstrate the validity of a long-period extension, independent estimates of peak ground displacement from recorded accelerograms and estimates of the seismic moment from distant recordings of earthquakes are shown to be in good agreement with the extended spectral amplitudes. The validity of a short-period extension has been also tested by comparing the values of pseudo acceleration spectral amplitudes at short periods with the recorded peak ground accelerations. The realistic nature of short- and long-period extensions provides additional tests for the accuracy of the present scaling relationships. Such relationships can thus be considered to provide a sound basis for macro- and micro-zoning specific to the highly seismic regions of western Himalaya and northeastern India.

1. Introduction

The concept of response spectrum in earthquake engineering was introduced by Biot [9], who also proposed the first response spectrum superposition method [10] to obtain an upper bound on the response of multi-degree-of-freedom (MDOF) structures. Since then, a large number of response spectrum superposition rules have been proposed by different investigators in a bid to achieve closer matching with the exact maximum response of MDOF structures with varying complexities ([113,22,69,76,82–84;20,5,86]; etc.) Important later developments relate to generalizing the response spectrum superposition method in order to gain statistical estimates of several significant peaks of the response amplitudes corresponding to the strong-motion stationary part of input ground excitation [30–35,37,39,4,40,41]. Presently, response spectrum methods are used extensively in earthquake-resistant design applications to characterize the design ground motion in terms of the response spectrum. Empirical scaling equations regarding all of the significant governing parameters, which can be assigned easily and accurately, are the most common method for describing the response spectrum amplitudes.

Trifunac [89] developed empirical scaling relations directly for Fourier spectrum (*FS*) amplitudes at different periods in terms of earthquake magnitude, epicentral distance, site geological condition, and component of motion. The same was then extended to the amplitudes of various types of response spectrum [101–103,91]. The site geology in these studies was defined qualitatively by a parameter s taking values of 0, 1, and 2 for sites on sediments, intermediate sites and geological basement rock sites, respectively. This was later refined to the depth h in km of the sedimentary deposits beneath the recoding station [105,106]. The attenuation with distance in all of these studies was defined by Richter's [75] attenuation function $A_0(R)$. In subsequent studies for attenuation of *FS* amplitudes [109,111], as well as the pseudo relative velocity (*PSV*) spectrum amplitudes [110,112], this was replaced by an improved frequency-dependent attenuation function $Att(\Delta, M, T)$ defined in terms of an equivalent source-to-site distance Δ, earthquake magnitude M, and the wave period T [107,108]. The next development [49–51,92–94] was to introduce the dependence on the site soil condition as defined qualitatively by a parameter s_L

* Corresponding author.
E-mail addresses: idgrh4@gmail.com (I.D. Gupta), trifunac@usc.edu (M.D. Trifunac).

https://doi.org/10.1016/j.soildyn.2017.12.005
Received 27 October 2017; Accepted 3 December 2017

taking on values of 0, 1, and 2 for sites on rock soil, stiff soil, and deep soil, respectively. Trifunac [95] has shown that the strong ground motion amplitudes depend significantly on both the local geological and site soil conditions. Yet another development was to define the effect of inhomogeneities along the propagation path by introducing the dependence of rock percentage along the source-to-site path in the empirical scaling relations [58,59].

Although all of the foregoing developments were specific to Southern California, they have also been applied to other parts of the world. Lee and Trifunac [56] developed the frequency-dependent attenuation function $Att(\Delta, M, T)$ for the former Yugoslavia and used it to generate empirical scaling relations for *FS* [57] and *PSV* [52] amplitudes. The scaling relations for the former Yugoslavia have been modified by developing an independent frequency-dependent attenuation function to describe the scaling of *FS* [63] and *PSV* [64] amplitudes from the deep focus and distant Vrancea earthquakes in Serbia. Gupta and Trifunac [38] have recently developed frequency-dependent attenuation functions and scaling relations for Fourier spectrum amplitudes for western Himalaya and northeastern India, which have been extended to the *PSV* amplitudes in the present work. The same functional form and regression method used for the *FS* amplitudes has also been adopted for the scaling of *PSV* amplitudes in this work, using the same database of 1236 components of accelerograms recorded in both regions of India.

Starting with the work of Johnson [44], a large number of scaling equations have been developed for the response spectrum amplitudes at different periods for various seismic regions around the world [21]; however, no worthwhile relationship is available for any part of India. A limited number of strong-motion data became available in India during the period of 1986–1999 from three isolated networks of about 40–50 analog accelerographs each—two operated in western Himalaya and one in the Shillong Plateau area of northeastern India [13]. This database formed the basis for a few models of ground motion peaks (e.g.; [14,72,79,85]). The first model for the scaling of *PSV* amplitudes was developed for northeast India by Das et al. [17] and used for the macrozonation of the region. However, due to the very limited database available, the authors combined the data from both shallow crustal and deep subduction earthquakes and could not include the dependence on site geological and soil conditions. Using 56 three-component accelerograms, Gupta [28] modified the attenuation relationship of Atkinson and Boore [8] to suit the ground motion amplitudes in northeastern India caused by Burmese subduction-zone earthquakes. This relationship showed a slower attenuation of pseudo spectral acceleration (*PSA*) amplitudes than the previous model of Das et al. [17]. Sharma et al. [80] proposed a scaling model for *PSA* amplitudes for the Himalayan region by using a larger database obtained by combining the data from the Zagros region in Iran. However, the similarity of the strong ground motion characteristics in the Himalaya and Zagros regions could not be justified. In addition, they considered only “rock” and “other” types of site conditions, which does not adequately describe the site effects.

In light of the previous discussion, most of the recent seismic hazard studies in India [18,47,7,70,71,77] have used arbitrarily selected ground motion prediction equations from other regions of the world rather than the available India-specific attenuation relationships. None of these studies performed any checks on the ability of the selected attenuation relations to describe the strong ground motion amplitudes in the area of interest in India. The reliability of such studies is thus questionable and difficult to assess. The scaling relations for *PSV* amplitudes proposed in this study for damping ratios $\varsigma = 0.00$, 0.02, 0.05, 0.10, and 0.20 will provide an improved basis to obtain a more reliable seismic hazard assessment specific to vast areas of western Himalaya and northeast India. The magnitude used in the present relations is the published magnitude, which can be defined directly without any requirement for empirical conversion into a specific magnitude type. In a hazard analysis, magnitude conversion is commonly a source of large uncertainties that are unaccounted for. Also, as discussed in our paper on Fourier spectra scaling [38], the use of moment magnitude is not appropriate for the scaling of high-frequency, strong-motion amplitudes between about 0.1 and 25 Hz. The distance used in our present scaling model is primarily the hypocentral distance, an estimation that does not involve the uncertainties usually associated with the estimation of fault-rupture distances, such as the closest distance to the fault- rupture plane or the surface projection of the rupture plane [24]. Further, the simple qualitative parameters used to define the site geological and soil conditions in the present scaling equations can capture the site amplification effects in a physically realistic manner, and it would be much easier to define these in practical applications.

Typical examples of the *PSV* spectra estimated from the proposed relations have illustrated that such spectra can account for the dependence on magnitude, distance, and recording site condition in a physically realistic and accurate way. The rate of growth of *PSV* amplitudes with magnitude is seen to slow down with an increase in magnitude, thus reaching a maximum beyond a certain magnitude that is larger for larger natural periods. Thus, the magnitude dependence is constrained in a very realistic manner. Also, the increase in spectral amplitudes is seen to slow down with a decrease in distance, which is the desired distance-saturation effect. Similar to the *FS* amplitudes [38], the *PSV* amplitudes are also seen to be larger on sediments compared to the basement rock at periods longer than about 0.24 s for all types of site soil conditions. However, unlike the *FS* amplitudes, the *PSV* amplitudes are larger on the stiff, as well as soft soil sites compared to rock soil in all periods. The *FS* amplitudes are seen to be higher on rock soil for periods below about 0.1 s. This can be considered as realistic behavior, because the high-frequency response spectral amplitudes also have significant contributions from lower frequencies. However, the amplification on soft soil sites is not seen to be that large at periods below 0.1 s. Finally, very good agreement will be shown to exist between the estimated and the actual response spectra of the recorded accelerograms.

To minimize the effects of the low- and high-frequency noise invariably present in the recorded strong-motion acceleration data, the proposed empirical relations for both western Himalaya and northeastern India are presented for the period range of 0.04 -3.0 s only. However, for the design of long structures, tall buildings, and structures on multiple distant supports, it becomes necessary to specify the design ground motion for much longer periods. Also, the design of equipment and stiff structures requires specifying the design ground motion at higher frequencies (short periods). The methods proposed by Trifunac [97,98] based on simple theoretical considerations is used in this work to show how the *PSV* spectral amplitudes can be extended to both long and short periods beyond the range within which the empirical scaling relations apply. The validity of such extrapolations for northeast India and western Himalaya has been tested and validated by comparing the estimates of seismic moment, peak ground displacement, and peak ground acceleration with other independent estimates of these quantities.

2. Strong-motion database used

The strong-motion database used for developing the empirical scaling relations for PSV amplitudes in this study is the same as detailed in Gupta and Trifunac [38] for developing similar relations for Fourier spectrum amplitudes. This includes 412 three-component accelerograms from 113 different earthquakes, from which 252 records are from 72 earthquakes in western Himalaya and 160 records from 41 earthquakes in northeastern India. Older analog, as well as later digital types of records, are considered in the database. Our database comprises 90 analog records (35 in western Himalaya and 55 in northeastern India) and 322 digital records (217 in western Himalaya and 105 in northeastern India). Analog data is recorded by 3 localized networks of 40–50 accelerographs operated by IIT Roorkee during the 1986–1999 period in the Kangra and Garhwal-Kumaon areas of western Himalaya

Table 1
Distribution of 148 Strong-Motion Records in Northestern India with Respect to Different Magnitude Intervals, Site Geology, and Local Soil Parameters.

Magnitude	$s = 0$ (sediments)				$s = 1$ (intermediate sites)				$s = 2$ (basement rock)			
	$s_L = 0$	$s_L = 1$	$s_L = 2$	All	$s_L = 0$	$s_L = 1$	$s_L = 2$	All	$s_L = 0$	$s_L = 1$	$s_L = 2$	All
4.0 – 4.9	0	0	39	39	0	0	1	1	3	0	2	5
5.0 – 5.9	2	1	40	43	0	3	13	16	4	7	12	23
6.0 – 6.9	0	0	15	15	0	0	1	1	3	0	2	5
All	2	1	94	97	0	3	15	18	10	7	16	33

Table 2
Distribution of 217 Strong-Motion Records in the Western Himalayan Region with Respect to Different Magnitude Intervals, Site Geology, and Local Soil Parameters.

Magnitude	$s = 0$ (sediments)				$s = 1$ (intermediate sites)				$s = 2$ (basement rock)			
	$s_L = 0$	$s_L = 1$	$s_L = 2$	All	$s_L = 0$	$s_L = 1$	$s_L = 2$	All	$s_L = 0$	$s_L = 1$	$s_L = 2$	All
4.0 – 4.9	3	11	37	51	0	0	3	3	15	19	22	56
5.0 – 5.9	2	6	36	44	0	0	5	5	3	19	13	35
6.0 – 6.9	0	0	1	1	0	0	0	0	0	6	16	22
All	5	17	74	96	0	0	8	8	18	44	51	113

and the Shillong Plateau area of northeast India [15,16] and the digital data is recorded by the National Strong Motion Instrumentation Network of about 300 modern digital accelerographs that have been operated by IIT Roorkee since 2005 [48]. The analog data are available in Shrikhande [81] and the digital data are available at IIT Rookee's website (http://www.pesmos.in) Details of the contributing earthquakes (date, time, epicentral location, focal depth, published magnitude, number of records, and earthquake name), as well as of the recording stations (station name and code, location, site soil parameters, site geology parameters, and brief geological description) for the strong-motion database used are given in Tables 1 and 2 in Gupta and Trifunac [38] and will not be repeated here.

2.1. Distribution of records

The locations of the recording stations and the contributing earthquakes for the present strong- motion data for western Himalaya and northeastern India are shown along with major tectonic features [19,25] in Figs. 1 and 2, respectively. Both of these regions are among the most seismically active areas in the world due to the presence of regional Himalayan tectonic features such main frontal thrust (MFT), the main boundary thrust (MBT), and the main central thrust (MCT). The tectonic features of the Burmese subduction zone (Burmese Boundary Fault, Naga-Disang Thrusts, etc.) and the Shillong Plateau area (Brahmputra, Dhubri, Kopili, etc. faults) additionally contributes to the seismicity of northeast India.

Records only with magnitude greater than or equal to 4.0 and hypocentral distances within 350 km are used in the present study. This reduces the total number of records from 412 to 365 with 217 records for the western Himalaya region from 47 earthquakes recorded at 80 stations and 148 records from 36 earthquakes recorded at 56 stations. Distributions of these records with respect to earthquake magnitude, focal depth, and hypocentral distance for both the western Himalayan and northeast Indian regions are shown in Fig. 3. The highest magnitude interval for both regions is from 6.5 to 7.0. The selected records show significant contributions from all the magnitude intervals, with the predominant magnitude range for western Himalaya from 4.5 to 5.5 and from 5.5 to 6.0 for northeast India. The records with magnitudes below 4.0 have high contamination from both low- and high-frequency noise and their inclusion was found to corrupt the results of the regression analysis. Also, the smaller magnitude values cannot be considered very reliable. The selected records are also seen to have significant contributions from all of the hypocentral distances with the majority of records in western Himalaya from a distance range of

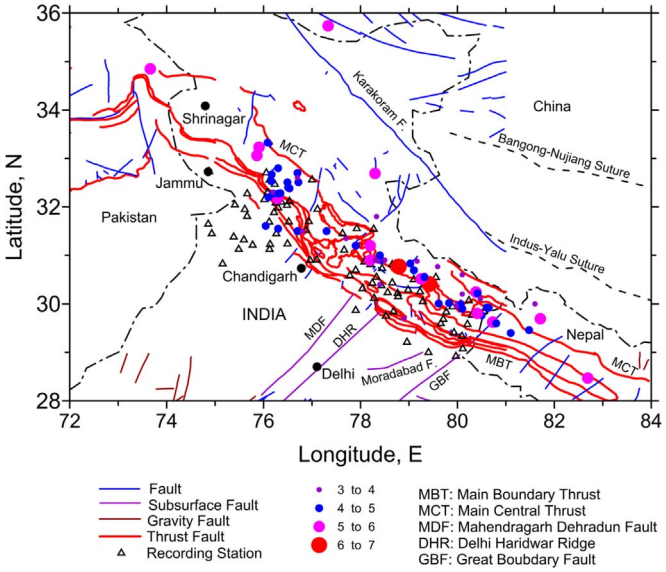

Fig. 1. The western Himalayan region with locations of recording stations (shown by triangles) and epicenters of contributing earthquakes (with magnitudes shown by different sizes and colors of filled circles). (For interpretation of the references to color in this figure legend, the reader is referred to the web version of this article.)

10–185 km and that in northeast India from a distance range of 35–205 km. The mean recording distances in western Himalaya and northeast India can approximately be taken as 100 km and 150 km, respectively. Records beyond 350 km are not considered because the distance attenuation functions developed in Gupta and Trifunac [38] could not be constrained properly by the inclusion of more distant records. The earthquakes in both regions are of shallow crustal origin, though a large number of the northeast Indian earthquakes is, in general, characterized by a somewhat deeper focal depth of more than 30 km compared to the within-20 km depth for western Himalayan earthquakes.

2.2. Local site conditions of recording stations

The site effects on strong earthquake ground motion depend significantly on both the site geology and local soil conditions [100,95]. Site geology refers to thick geological strata of the order of kilometers, whereas local soil condition is described by strata of soil within the top

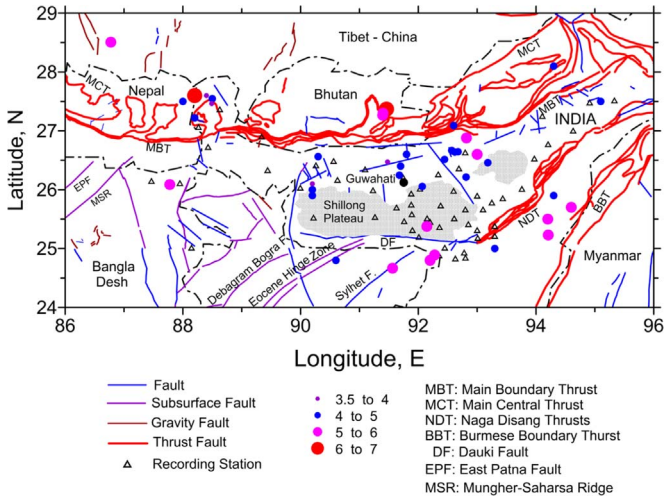

Fig. 2. The northeast Indian region with locations of recording stations (shown by triangles) and epicenters of contributing earthquakes (with magnitudes shown by different sizes and colors of filled circles). (For interpretation of the references to color in this figure legend, the reader is referred to the web version of this article.)

100–200 m of the ground surface [100,99]. Following our study on Fourier spectrum amplitudes [38], the site geology and soil conditions are defined qualitatively using indicator variables s and s_L, respectively. The site geology parameter s takes on values of 0, 1, and 2 for sites on sedimentary deposits, intermediate rocks, or complex geological environments that cannot be categorized unambiguously, and geological basement rocks, respectively [104]. On the other hand, the site soil parameter s_L takes on values of 0, 1, and 2 for sites on rock soil, stiff soil, and deep soil, respectively [92–94]. As per Trifunac [99], rock soil sites are considered to be those in which the shear wave velocity is less than 800 m/s only in the top 10 m of the ground surface, whereas the stiff soil and deep soil sites are those in which the shear wave velocity is less than 800 m/s in the top ~ 75 m and 150–200 m, respectively. The values of these parameters for all 136 stations at which the strong-motion data considered in this study are adopted from our study for the Fourier spectrum amplitudes [38].

Fig. 4(a) and (b) show the distribution of 148 three-component records considered for northeastern India and 217 records for western Himalaya with magnitudes greater than or equal to 4.0 with respect to three local soil conditions defined by parameter s_L (= 0, 1 and 2) for each of the three site geologic conditions defined by parameter s (= 0, 1 and 2). The majority of records in both regions are seen to belong the sediments ($s = 0$) and deep soil ($s_L = 2$) site types, followed by basement rock ($s = 2$) and deep soil ($s_L = 2$) site types. The total number of records with intermediate types of geology ($s = 1$) is comparatively small, most of which belong to deep soil site types. A few records in both northeast India and western Himalaya also belong to the unexpected combination of sediments ($s = 0$) and rock soil ($s_L = 0$) type of site condition, which may represent the sites with outcrops in an area otherwise covered by sediments.

Tables 1 and 2 give the distribution of the data shown in Fig. 4 among three different magnitude intervals (4.0–4.9, 5.0–5.9, and 6.0–6.9) for northeastern India and western Himalaya, respectively. The maximum number of records for all site categories in northeastern India are given by earthquakes in the magnitude range of 5.0–5.9, whereas that in western Himalaya by earthquakes in the magnitude range of 4.0–4.9. None of the data in either region are distributed uniformly among various magnitude intervals with respect to site geological and local soil conditions. To eliminate the possible bias in the scaling relations developed from this non-uniform distribution of data, a decimation scheme is adopted following Trifunac and Anderson [101] before data is used in the regression analysis.

3. Development of scaling relations

The scaling relations developed in this study for the pseudo relative velocity spectrum amplitudes $PSV(T)$ for the five ratios of critical damping $\zeta = 0.00$, 0.02, 0.05, 0.10, and 0.20 are similar to those developed recently by Gupta and Trifunac [38] for the Fourier amplitude spectra in northeastern India and western Himalaya. The frequency-dependent attenuation functions developed for these two regions are used to perform the regression directly for the dependence of PSV amplitudes on magnitude, site geological condition, and the local soil condition. The form of the regression equation is the same as what we used for the Fourier Spectrum amplitudes; that is,

$$\log_{10}PSV(T) = M + A_0(T)\log_{10}\Delta + C_1(T) + C_2(T)M + C_3(T)M^2 + C_4(T)v + C_5(T)s + C_6^0(T)S_L^0 + C_6^1(T)S_L^1 + C_6^2(T)S_L^2 \quad (1)$$

Here, $PSV(T)$ represents the pseudo relative velocity spectrum amplitude at a natural period of the structure T for a specific damping ratio, M denotes the earthquake magnitude, v denotes the component of motion (v= 0 for horizontal and 1 for vertical component), s denotes the site geology parameter ($s = 0$ for alluvium, 1 for intermediate sites, and 2 for basement rocks), and S_L^0, S_L^1, and S_L^2 are variables taking on the value of 1 for the site soil parameters $s_L = 0$, 1, and 2 representing rock soil, stiff soil, deep soil, respectively, and zero otherwise. The coefficients $C_1(T)$, $C_2(T)$, $C_3(T)$, $C_4(T)$, $C_5(T)$, $C_6^0(T)$, $C_6^1(T)$, and $C_6^2(T)$ are the period-dependent scaling functions.

The scaling model of Eq. (1) is similar to that of Trifunac and coworkers for the California region [49–51,92–94]. A common dependence of PSV amplitudes in western Himalaya and northeastern India on earthquake magnitude, site geology, and site soil condition is assumed, which has been found to be consistent with the recorded data. Also, the same equation will be used for both horizontal and vertical motions contrary to the separate equations in some past studies (e.g., [1,2,3]). This is justified on the grounds that two components of any motion should have an identical dependence on magnitude, distance, and site conditions [53].

In Eq. (1), $A_0(T)\log_{10}\Delta$ is the frequency-dependent attenuation function used in Gupta and Trifunac [38] with Δ as the representative source-to-site distance, defined by

$$\Delta = S\left(ln\frac{R^2 + H^2 + S^2}{R^2 + H^2 + S_0^2}\right)^{-\frac{1}{2}}, \quad (2)$$

with S_0 as the correlation radius of the source, S the (magnitude-dependent) fault size, and H the focal depth. The correlation radius S_0 is given by [42]

$$S_0 = min\left(\frac{\beta T}{2}, \frac{S}{2}\right). \quad (3)$$

where β is the shear wave velocity at the earthquake source taken equal to 3.5 km/s for northeastern India and 3.3 km/s for western Himalaya, following Gupta and Trifunac [38]. The fault size S (in km) is approximated empirically to be a linear function of the earthquake magnitude M, as follows [38]:

$$S = \begin{cases} 0.2 \, for \, M \le 3.0 \\ -13.557 + 4.586M \text{ for } 3.0 < M \le 6.0 \\ 13.959 \text{ for } M > 6.0 \end{cases} \quad (4)$$

Fig. 5 shows the attenuation function $A_0(T)$ for northeastern India and western Himalaya from Gupta and Trifunac [38] compared with the corresponding attenuation function for Southern California [108,55], the former Yugoslavia [56], and the Vrancea earthquakes in Serbia [63–68]. The attenuation in northeastern India is slower at all the periods compared to that in western Himalaya, California, the former Yugoslavia, and Vrancea. Although the western Himalayan attenuation is not much different from those for the former Yugoslavia

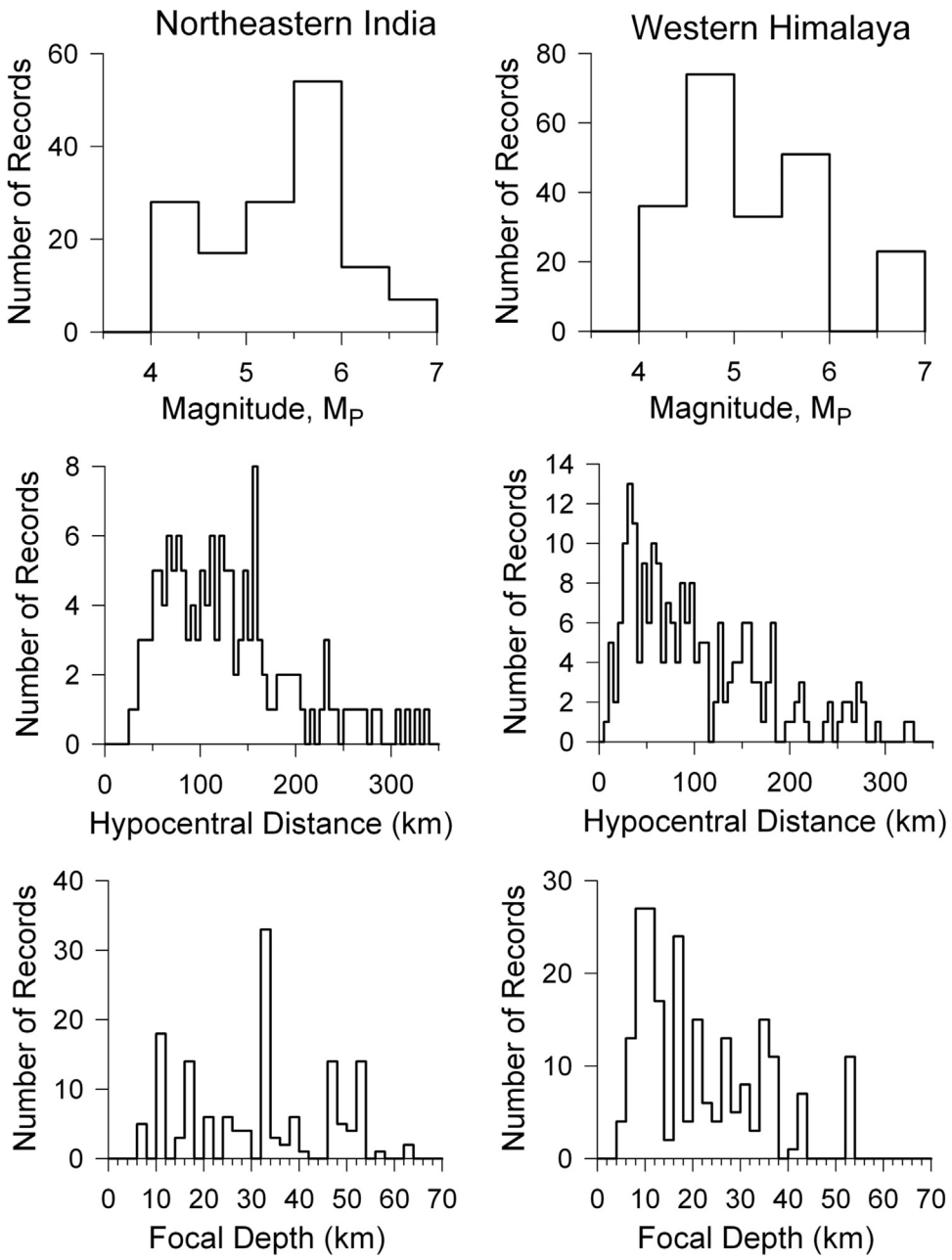

Fig. 3. The distributions of strong-motion records by earthquakes with magnitudes greater than or equal to 4.0 and a hypocentral distance within 350 km, with respect to magnitude (top plots), hypocentral distance (middle plots), and focal depth (bottom plots). Plots on the right are for western Himalaya and for northeast India on the left.

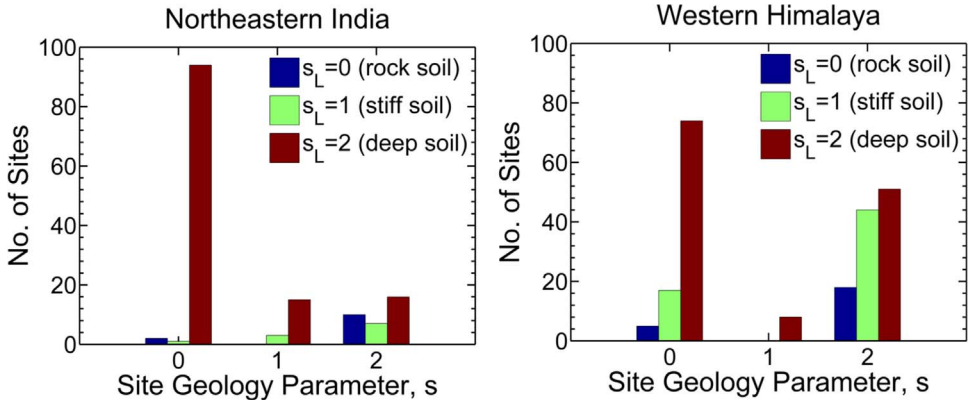

Fig. 4. The distributions of strong-motion records considered in this study for northeastern India (left-side plot) and western Himalaya (right-side plot) with respect to site geologic and local soil conditions.

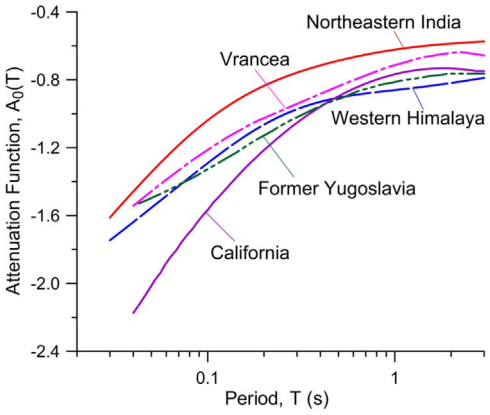

Fig. 5. The attention functions of western Himalaya, northeastern India, California, the former Yugoslavia, and Romanian earthquakes in Vrancea (adopted from [38]).

and Vrancea up to about 0.5 s periods, it is faster for longer periods. The attenuation functions for northeast India and western Himalaya are thus quite specific to these regions, and the use of ground motion prediction equations from other parts of the world may not be appropriate for these highly seismic regions of India. The values of the attenuation functions $A_0^E(T)$ and $A_0^W(T)$ for northeastern India and western Himalaya as developed by Gupta and Trifunac [38] are given in Table 3 for 13 selected periods between 0.04 s and 3.0 s. The 13 periods are considered sufficient to define the smoothed attenuation functions for most practical applications, because the value for any other period in the range 0.04–3.0 s can be obtained with good accuracy by interpolation.

3.1. Regression analysis and scaling functions

Using the attenuation functions shown in Fig. 5 and listed in Table 3 for the northeast Indian and western Himalayan regions, the various scaling functions in the relationship of Eq. (1) are estimated by regression analysis of the *PSV* amplitudes for the selected database of 1095 accelerogram components. Before computation of *PSV* spectra, the analog accelerograms were processed for instrument correction [88] and both analog and digital accelerograms were processed for baseline correction [87]. The details of the procedure used for processing of the accelerograms is given in Gupta [29]. Further, for use in the regression analysis, the *PSV* amplitudes at each period are decimated to minimize any possible bias due to uneven distribution of data among different magnitude ranges, site geology condition parameters, and site soil condition parameters for both horizontal and vertical components of motion [101]. For this purpose, all 1095 spectral amplitudes at each period are grouped into three magnitude ranges of 4.0–4.9, 5.0–5.9, and 6.0–6.9. The amplitudes in each magnitude group are then separated sequentially as per the component of motion v (= 0, 1), site geology parameter s (= 0, 1 and 2), and site soil parameter s_L (= 0, 1 and 2). The amplitudes in each of the 54 sub-divisions thus created are then arranged in increasing order of $PSV(T)$ values. A maximum of 33 values are finally included in the regression analysis from each group, which corresponds to the serial numbers closest to the 3rd, 6th, 9th, ….., 96th and 99th percentile positions. The number of thus decimated data points varies with the period, due to lower and higher cutoff periods for each accelerogram.

By adopting the frequency-dependent attenuation functions for northeast India and western Himalaya from Gupta and Trifunac [38], the various scaling functions in the relationship of Eq. (1) are estimated by adopting a two-step weighted regression analysis procedure [78]. In the first step, the decimated data for each period is used to fit the following equation by a least-squares regression analysis:

$$\log_{10}PSV(T) - M - A_0^E(T)[(\log\Delta)\delta_E] - A_0^W(T)[(\log\Delta)\delta_W] = C_4(T)v + C_5(T)s + \sum_{j=1}^{J} B_j(T)e_j \quad (5)$$

In this equation, $A_0^E(T)$ and $A_0^W(T)$ are the frequency-dependent attenuation functions and δ_W and δ_E are the indicator variables for the northeast Indian and western Himalayan regions, respectively. These are assigned a value of 1.0 for the data points belonging to the respective region and 0.0 otherwise. The e_j is also an indicator variable assigned a value of 1.0 if the data belongs to the jth earthquake and 0.0 otherwise.

Using the regression coefficients $B_j(T)$ obtained by the fitting of Eq. (5), the magnitude dependence is obtained in the second step by weighted least-squares regression analysis on the following equation:

$$B_j(T) = C_1^E(T)\delta_E + C_1^W(T)\delta_W + C_2(T)M_j + C_3(T)M_j^2. \quad (6)$$

The weight w_j for the jth equation is taken equal to $(\sigma_1^2/n_j + \sigma_2^2)^{-1}$ with σ_1^2 and σ_2^2 as the variances of the fitting of Eqs. (5) and (6) and n_j as the number of spectral amplitudes used for the jth earthquake [45]. As σ_2^2 is not known in advance, an iterative procedure is followed in the second step by starting with a value of σ_2^2 equal to zero and increasing it in small steps. The convergence is indicated by the weighted variance of the fitting of Eq. (6) close to 1.0 [78].

The estimated regression coefficients $C_4(T)$ and $C_5(T)$ in Eq. (5) and the coefficients $C_1^E(T)$, $C_1^W(T)$, $C_2(T)$, and $C_3(T)$ in Eq. (6) show a fluctuating nature when plotted versus period T. For the predicted *PSV* spectra to have physically realistic trends and variations, it is necessary that the regression coefficients are smoothed. The smoothed regression coefficients are designated by $\hat{C}_4(T)$, $\hat{C}_5(T)$, $\hat{C}_1^E(T)$, $\hat{C}_1^W(T)$, $\hat{C}_2(T)$, and $\hat{C}_3(T)$, respectively. To develop the complete scaling relationship of Eq. (1), the smoothed scaling coefficients are used to develop the dependence on the site soil condition jointly for northeast India and western Himalaya by a least-squares fitting of the following equation:

$$\log_{10}PSV(T) - M - A_0^E(T)[(\log\Delta)\delta_E] - A_0^W(T)[(\log\Delta)\delta_W] - \hat{C}_1^E(T)\delta_E - \hat{C}_1^W(T)\delta_W - \hat{C}_2(T)M - \hat{C}_3(T)M^2 - \hat{C}_4(T)v + \hat{C}_5(T)s \cdot = C_6^0(T)S_L^0 + C_6^1(T)S_L^1 + C_6^2(T)S_L^2 \quad (7)$$

Due to limited data for the rock soil (s_L = 0) and stiff soil (s_L = 1), all 1095 data points are used for developing the dependence on local soil conditions rather than the decimated data only. The estimated coefficients $C_6^0(T)$, $C_6^1(T)$ and $C_6^2(T)$ have also been smoothed and the resulting coefficients are designated by $\hat{C}_6^0(T)$, $\hat{C}_6^1(T)$, and $\hat{C}_6^2(T)$, respectively.

The foregoing regression analysis has been performed for the $PSV(T)$ amplitudes at 63 periods T between 0.04 s and 3.0 s and five ratios of critical damping: ζ = 0.00, 0.02, 0.05, 0.10, and 0.20. Typical results on the variations of both the original and the smoothed regression coefficients $C_1^E(T)$, $C_1^W(T)$, $C_2(T)$, $C_3(T)$, and $C_4(T)$ that define the dependence on earthquake magnitude and component of motion for damping ratio ζ = 0.05 are shown in Fig. 6. The coefficients $C_1^E(T)$ and

Table 3
Frequency-dependent Attenuation Functions $A_0^E(T)$ and $A_0^W(T)$ for Northeastern India and Western Himalaya at 13 Selected Periods T from [38].

T (s)	0.04	0.06	0.08	0.10	0.15	0.20	0.40	0.60	0.80	1.0	1.5	2.0	3.0
$-A_0^E(T)$	1.45785	1.25504	1.12609	1.03811	0.90710	0.83529	0.71489	0.66683	0.63963	0.62226	0.59845	0.58661	0.57433
$-A_0^W(T)$	1.63821	1.48400	1.37414	1.29028	1.14894	1.06385	0.92924	0.89051	0.87250	0.86043	0.83735	0.81835	0.78843

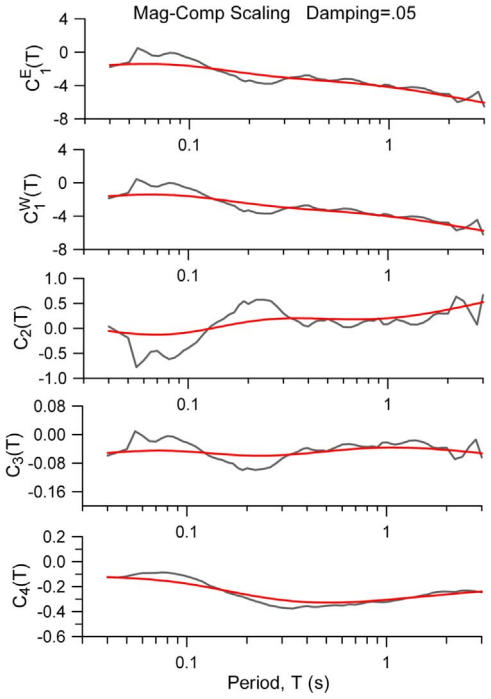

Fig. 6. Typical results for the original and smoothed regression coefficients defining the dependence of *PSV* amplitudes for $\zeta = 0.05$ on magnitude M and component of motion parameter v as in Eqs. (5) and (6).

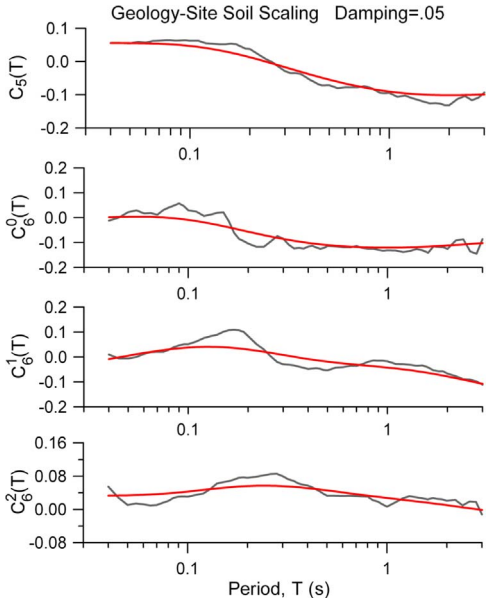

Fig. 7. Typical results for the original and smoothed regression coefficients defining the dependence of *PSV* amplitudes for $\zeta = 0.05$ on site geological parameter s and site soil condition parameter s_L as in Eqs. (5) and (7).

$C_1^W(T)$ represent the relative source strength effects for northeast India and western Himalaya, respectively. All the other coefficients are obtained to be common to both regions. The coefficients $C_2(T)$ and $C_3(T)$ define the dependence on M and M^2, and coefficient $C_4(T)$ accounts for the dependence on the component of motion parameter v. The coefficient of M^2 as negative and significantly different from zero accounts for the magnitude saturation effects. Fig. 7 shows the original and smoothed coefficient $C_5(T)$ for the dependence on site geology parameter s and the coefficients $C_6^0(T)$, $C_6^1(T)$, and $C_6^2(T)$ defining the dependence on the site soil condition parameter s_L for $\zeta = 0.05$. The results for other damping ratios are similar to those shown in Figs. 6 and 7.

Values of the smoothed coefficients $\hat{C}_1^E(T)$, $\hat{C}_1^W(T)$, $\hat{C}_2(T)$, $\hat{C}_3(T)$, $\hat{C}_4(T)$, $\hat{C}_5(T)$, $\hat{C}_6^0(T)$, $\hat{C}_6^1(T)$, and $\hat{C}_6^2(T)$ at 13 selected periods between 0.04 s and 3.0 s for all the five values of damping ratio are given in Tables 4.1–4.5.

3.2. Statistics of PSV residues

The smoothed regression coefficients given in Tables 4.1–4.5 can be used to obtain the least-squares smoothed estimates of the pseudo relative velocity spectrum, $P\hat{S}V(T)$, for any of the five damping ratios using the prediction relationship of Eq. (1), which can be written for northeast India and the western Himalaya as follows:

$$\begin{aligned}\log_{10}P\hat{S}V(T) &= M + A_0^E(T)\log\Delta + \hat{C}_1^E(T) + \hat{C}_2(T)M \\ &\quad + \hat{C}_3(T)M^2 + \hat{C}_4(T)v + \hat{C}_5(T)s \\ &\quad + C_6^0(T)S_L^0 + C_6^1(T)S_L^1 + C_6^2(T)S_L^2 \end{aligned} \tag{8a}$$

and

$$\begin{aligned}\log_{10}P\hat{S}V(T) &= M + A_0^W(T)\log\Delta + \hat{C}_1^W(T) + \hat{C}_2(T)M \\ &\quad + \hat{C}_3(T)M^2 + \hat{C}_4(T)v + \hat{C}_5(T)s \\ &\quad + C_6^0(T)S_L^0 + C_6^1(T)S_L^1 + C_6^2(T)S_L^2 \end{aligned} \tag{8b}$$

where superscripts E and W represent northeast India and western Himalaya, respectively. For a given period T and specified values of the parameters s, v, s_L and Δ, the $\log_{10}P\hat{S}V(T)$ in both of the above equations represent a parabola as a function of magnitude M. Following Trifunac and colleagues [101–103,110,112,91], it is assumed that the scaling relations of Eq. (8a) and (8b) apply only in the range of $M_{\min}(T) \le M \le M_{\max}(T)$, where

$$M_{\max}(T) = -(1 + \hat{C}_2(T))/2\hat{C}_3(T) \text{and} M_{\min}(T) = -\hat{C}_2(T)/2\hat{C}_3(T). \tag{9}$$

For $M \le M_{\min}(T)$, the value of M in the terms $\hat{C}_2(T)M + \hat{C}_3(T)M^2$ in Eq. (8a) and (8b) is replaced by $M_{\min}(T)$. For $M \ge M_{\max}(T)$, $M_{\max}(T)$ is used for M in all the terms in Eq. (8a) and (8b). Thus, $\log_{10}P\hat{S}V(T)$ increases linearly with M for $M \le M_{\min}(T)$, parabolically for $M_{\min}(T) \le M \le M_{\max}(T)$, and attains a constant value corresponding to $M_{\max}(T)$ for $M \ge M_{\max}(T)$.

The residues $\in(T)$ at each period are defined by the differences between the pseudo relative velocity spectrum amplitudes $PSV(T)$ computed from the recorded accelerograms and the least-squares estimates $P\hat{S}V(T)$ obtained from Eq. (8a) and (8b) as

$$\in(T) = \log_{10}PSV - \log_{10}P\hat{S}V(T). \tag{10}$$

The residuals thus describe the distribution of the observed $PSV(T)$ about the estimate $P\hat{S}V(T)$. The distribution of $\in(T)$, as in Trifunac and colleagues [110,112,49–51] can be described by the following probability distribution function with parameters $\alpha(T)$, $\beta(T)$ and $N(T)$ at each period T:

$$p(\in,T) = [1 - \exp(-\exp(\alpha(T)\in(T) + \beta(T)))]^{N(T)}, \tag{11}$$

where $p(\in,T)$ represents the probability that $\log_{10}PSV(T) - \log_{10}P\hat{S}T(T) \le \in(T)$. The integer power $N(T)$ is defined by the empirical relation

$$N(T) = \min(10, [25/T]), \tag{12}$$

with $[25/T]$ as the integer part of $25/T$. The parameters $\alpha(T)$ and $\beta(T)$ are then estimated by fitting the probability distribution of Eq. (11) and rewriting it as follows:

$$\ln(-\ln(1 - p^{1/N(T)})) = \alpha(T)\in(T) + \beta(T). \tag{13}$$

For a given value of residual $\in(T)$ at period T, the actual probability that $\in(T)$ will not be exceeded is defined, as the fraction of the residues that are smaller than the given value. Typical examples of the residues $\in(T)$ corresponding to the probabilities $p = 0.1, 0.2, \ldots, 0.9$ for $\zeta = 0.05$ are given in Figs. 8 and 9 for northeast India and western

Table 4.1
Smoothed Regression Coefficients and Statistical Parameters of Residues for the Scaling Models of Eqs. (8a) and (8b).

T (s)	0.04	0.06	0.08	0.10	0.15	0.20	0.40	0.60	0.80	1.0	1.5	2.0	3.0
Regression Coefficients for Scaling of PSV With $\zeta = 0.00$													
$\hat{C}_1^E(T)$	0.0165	−0.5511	−1.0197	−1.4297	−2.2085	−2.7121	−3.6409	−4.1431	−4.6973	−4.8438	−5.3747	−5.6977	−6.0929
$\hat{C}_1^W(T)$	−0.1575	−0.6342	−1.0477	−1.4245	−2.1674	−2.6612	−3.5770	−4.0517	−4.5557	−4.6859	−5.1445	−5.4100	−5.7205
$\hat{C}_2(T)$	−0.3968	−0.2405	−0.1093	0.0053	0.2123	0.3277	0.4489	0.4763	0.5139	0.5246	0.5568	0.5640	0.5559
$\hat{C}_3(T)$	−0.0317	−0.0414	−0.0498	−0.0572	−0.0696	−0.0751	−0.0727	−0.0673	−0.0635	−0.0628	−0.0601	−0.0576	−0.0529
$\hat{C}_4(T)$	0.0589	0.0127	−0.0282	−0.0666	−0.1459	−0.2005	−0.2806	−0.2862	−0.2706	−0.2644	−0.2373	−0.2170	−0.1887
$\hat{C}_5(T)$	0.0868	0.0798	0.0716	0.0621	0.0366	0.0130	−0.0489	−0.0786	−0.0984	−0.1017	−0.1070	−0.1043	−0.0952
$\hat{C}_6^0(T)$	0.0265	0.0463	0.0486	0.0401	0.0044	−0.0285	−0.0906	−0.1069	−0.1132	−0.1139	−0.1135	−0.1107	−0.1046
$\hat{C}_6^1(T)$	0.0148	0.0573	0.0794	0.0884	0.0827	0.0635	0.0019	−0.0234	−0.0408	−0.0452	−0.0658	−0.0853	−0.1174
$\hat{C}_6^2(T)$	0.0299	0.0550	0.0709	0.0809	0.0917	0.0924	0.0738	0.0573	0.0418	0.0379	0.0225	0.0103	−0.0088
Statistical Parameters for Distribution of Residuals for Northeast India													
$\hat{\alpha}(T)$	1.3091	1.2716	1.2507	1.2388	1.2244	1.2155	1.1715	1.1228	1.0646	1.0494	0.9943	0.9583	0.9782
$\hat{\beta}(T)$	1.0208	1.0090	1.0015	0.9962	0.9875	0.9818	0.9711	0.9698	0.9752	0.9778	0.9915	1.0036	0.9377
$N(T)$	10	10	10	10	10	10	10	10	10	10	10	10	8
Statistical Parameters for Distribution of Residuals for Western Himalaya													
$\hat{\alpha}(T)$	1.1596	1.1758	1.1851	1.1902	1.1955	1.1970	1.1968	1.1987	1.2123	1.2197	1.2717	1.3373	1.5848
$\hat{\beta}(T)$	0.9782	0.9529	0.9383	0.9311	0.9293	0.9363	0.9631	0.9743	0.9819	0.9838	0.9931	1.0023	0.9359
$N(T)$	10	10	10	10	10	10	10	10	10	10	10	10	8

Table 4.2
Smoothed Regression Coefficients and Statistical Parameters of Residues for the Scaling Models of Eqs. (8a) and (8b).

T (s)	0.04	0.06	0.08	0.10	0.15	0.20	0.40	0.60	0.80	1.0	1.5	2.0	3.0
Regression Coefficients for Scaling of PSV With $\zeta = 0.02$													
$\hat{C}_1^E(T)$	−1.0822	−1.0956	−1.2475	−1.4813	−2.0885	−2.5454	−3.3811	−3.7904	−4.2762	−4.4183	−5.0078	−5.4478	−6.0756
$\hat{C}_1^W(T)$	−1.1514	−1.1081	−1.2245	−1.4357	−2.0157	−2.4632	−3.2842	−3.6719	−4.1194	−4.2488	−4.7808	−5.1733	−5.7290
$\hat{C}_2(T)$	−0.1838	−0.1978	−0.1620	−0.0986	0.0630	0.1692	0.2699	0.2736	0.2999	0.3129	0.3817	0.4417	0.5316
$\hat{C}_3(T)$	−0.0418	−0.0400	−0.0421	−0.0464	−0.0564	−0.0616	−0.0574	−0.0498	−0.0451	−0.0447	−0.0454	−0.0476	−0.0517
$\hat{C}_4(T)$	−0.0896	−0.1062	−0.1267	−0.1502	−0.2061	−0.2479	−0.3116	−0.3137	−0.2965	−0.2901	−0.2627	−0.2428	−0.2154
$\hat{C}_5(T)$	0.0606	0.0594	0.0559	0.0504	0.0322	0.0132	−0.0416	−0.0699	−0.0903	−0.0941	−0.1023	−0.1025	−0.0980
$\hat{C}_6^0(T)$	0.0127	0.0202	0.0184	0.0105	−0.0174	−0.0429	−0.0950	−0.1109	−0.1172	−0.1176	−0.1145	−0.1086	−0.0973
$\hat{C}_6^1(T)$	−0.0146	0.0193	0.0390	0.0493	0.0523	0.0419	−0.0023	−0.0232	−0.0389	−0.0430	−0.0628	−0.0817	−0.1131
$\hat{C}_6^2(T)$	0.0290	0.0369	0.0440	0.0503	0.0612	0.0655	0.0569	0.0440	0.0314	0.0283	0.0167	0.0078	−0.0060
Statistical Parameters for Distribution of Residuals for Northeast India													
$\hat{\alpha}(T)$	1.4370	1.3540	1.3074	1.2798	1.2466	1.2312	1.1886	1.1430	1.0812	1.0633	0.9897	0.9345	0.9229
$\hat{\beta}(T)$	0.9215	0.9373	0.9442	0.9466	0.9455	0.9429	0.9420	0.9489	0.9627	0.9675	0.9893	1.0069	0.9482
$N(T)$	10	10	10	10	10	10	10	10	10	10	10	10	8
Statistical Parameters for Distribution of Residuals for Western Himalaya													
$\hat{\alpha}(T)$	1.3017	1.3128	1.3116	1.3034	1.2759	1.2530	1.2168	1.2153	1.2298	1.2368	1.2795	1.3275	1.5264
$\hat{\beta}(T)$	0.9838	0.9616	0.9474	0.9387	0.9318	0.9346	0.9551	0.9658	0.9733	0.9751	0.9830	0.9901	0.9175
$N(T)$	10	10	10	10	10	10	10	10	10	10	10	10	8

Himalaya, respectively. The rough solid curves represent the actual residues for each probability level, and the smooth solid curves are obtained by smoothing the rough curves along the period axes. The smooth dashed curves are the residues estimated from the distribution function of Eq. (11), with the parameters $\hat{\alpha}(T)$ and $\hat{\beta}(T)$ obtained by the least-squares fitting of Eq. (13) to the smoothed curves $\hat{p}(\in,T)$ shown in Figs. 8 and 9 and parameter $N(T)$ defined by Eq. (12). It is seen that the values of the residues estimated from the distribution function of Eq. (11) can approximate the smooth observed residues very well for all nine probability levels of 0.1 through 0.9. This is further confirmed by performing the chi-square (χ^2) and the Kolmogorov–Smirnov (K-S) statistical tests as in Trifunac [92] and described in the next paragraph.

The statistical parameters $N(T)$, $\hat{\alpha}(T)$, and $\hat{\beta}(T)$ used to describe the probability distribution of the pseudo spectral velocity residues, illustrated for $\zeta = 0.05$, are plotted in Figs. 10 and 11 for northeastern India and western Himalaya, respectively. To show that the distribution function of Eq. (11) with these parameters can be used to describe the residuals, the bottom two full curves in Figs. 10 and 11 show the smoothed amplitudes of K-S(T) and $\chi^2(T)$, respectively. The corresponding dashed curves are their respective 95% cutoff levels for rejecting the hypothesis that the residuals follow the distribution function of Eq. (11). It is seen that with the exception of a limited period ranges near the lower- and upper-period ends for northeast India, both the K-S and the χ^2 tests fail to reject the H_0 hypothesis at the 95% confidence level. Similar observations were made for the *PSV* amplitudes for other damping ratios. Hence, the distribution of Eq. (11) is accepted to describe the distribution of the residuals of the *PSV* spectrum in this paper. The values of the parameters $N(T)$, $\hat{\alpha}(T)$, and $\hat{\beta}(T)$ for both northeast India and western Himalaya are also given at 13 selected periods in Tables 4.1– 4.5 for the 5 damping ratios, along with the regression coefficients in Eq. (8a) and (8b).

With the statistical parameters $N(T)$, $\hat{\alpha}(T)$, and $\hat{\beta}(T)$, the distribution function of Eq. (11) can be used to estimate the values, $\in_p(T)$,

Table 4.3
Smoothed Regression Coefficients and Statistical Parameters of Residues for the Scaling Models of Eqs (8a) and (8b).

T (s)	0.04	0.06	0.08	0.10	0.15	0.20	0.40	0.60	0.80	1.0	1.5	2.0	3.0
Regression Coefficients for Scaling of PSV With $\zeta = 0.05$													
$\hat{C}_1^E(T)$	−1.5180	−1.4032	−1.4672	−1.6376	−2.1481	−2.5531	−3.2837	−3.6180	−4.0403	−4.1739	−4.7840	−5.2937	−6.0709
$\hat{C}_1^W(T)$	−1.5865	−1.4157	−1.4445	−1.5924	−2.0750	−2.4694	−3.1818	−3.4950	−3.8831	−4.0056	−4.5652	−5.0329	−5.7458
$\hat{C}_2(T)$	−0.0532	−0.1193	−0.1185	−0.0798	0.0456	0.1336	0.2016	0.1832	0.1927	0.2043	0.2869	0.3762	0.5255
$\hat{C}_3(T)$	−0.0515	−0.0456	−0.0450	−0.0473	−0.0547	−0.0585	−0.0521	−0.0428	−0.0367	−0.0362	−0.0381	−0.0429	−0.0522
$\hat{C}_4(T)$	−0.1239	−0.1380	−0.1559	−0.1765	−0.2264	−0.2644	−0.3240	−0.3268	−0.3111	−0.3053	−0.2801	−0.2622	−0.2382
$\hat{C}_5(T)$	0.0554	0.0547	0.0518	0.0469	0.0304	0.0128	−0.0389	−0.0662	−0.0865	−0.0903	−0.0996	−0.1013	−0.0992
$\hat{C}_6^0(T)$	0.0014	0.0036	−0.0004	−0.0086	−0.0339	−0.0562	−0.1011	−0.1146	−0.1197	−0.1199	−0.1168	−0.1115	−0.1016
$\hat{C}_6^1(T)$	−0.0082	0.0164	0.0308	0.0382	0.0396	0.0304	−0.0077	−0.0253	−0.0384	−0.0420	−0.0599	−0.0776	−0.1075
$\hat{C}_6^2(T)$	0.0332	0.0352	0.0387	0.0429	0.0518	0.0562	0.0512	0.0409	0.0303	0.0277	0.0178	0.0102	−0.0015
Statistical Parameters for Distribution of Residuals for Northeast India													
$\hat{\alpha}(T)$	1.4791	1.3913	1.3397	1.3073	1.2640	1.2419	1.1924	1.1507	1.0935	1.0760	1.0000	0.9399	0.9211
$\hat{\beta}(T)$	0.9244	0.9414	0.9484	0.9502	0.9473	0.9433	0.9412	0.9488	0.9637	0.9688	0.9925	1.0117	0.9559
$N(T)$	10	10	10	10	10	10	10	10	10	10	10	10	8
Statistical Parameters for Distribution of Residuals for Western Himalaya													
$\hat{\alpha}(T)$	1.2849	1.3135	1.3223	1.3194	1.2950	1.2698	1.2213	1.2139	1.2240	1.2294	1.2612	1.2936	1.4535
$\hat{\beta}(T)$	0.9808	0.9610	0.9477	0.9393	0.9320	0.9339	0.9522	0.9622	0.9694	0.9711	0.9784	0.9848	0.9100
$N(T)$	10	10	10	10	10	10	10	10	10	10	10	10	8

Table 4.4
Smoothed Regression Coefficients and Statistical Parameters of Residues for the Scaling Models of Eqs. (14a) and (14b).

T (s)	0.04	0.06	0.08	0.10	0.15	0.20	0.40	0.60	0.80	1.0	1.5	2.0	3.0
Regression Coefficients for Scaling of PSV With $\zeta = 0.10$													
$\hat{C}_1^E(T)$	−1.7120	−1.7103	−1.7837	−1.9043	−2.2467	−2.5360	−3.1590	−3.4838	−3.8876	−4.0165	−4.6227	−5.1492	−5.9706
$\hat{C}_1^W(T)$	−1.7841	−1.7297	−1.7697	−1.8684	−2.1813	−2.4566	−3.0534	−3.3568	−3.7292	−3.8482	−4.4098	−4.8994	−5.6647
$\hat{C}_2(T)$	0.0031	−0.0353	−0.0395	−0.0241	0.0350	0.0807	0.1206	0.1096	0.1223	0.1343	0.2222	0.3213	0.4914
$\hat{C}_3(T)$	−0.0555	−0.0516	−0.0503	−0.0506	−0.0524	−0.0530	−0.0455	−0.0375	−0.0322	−0.0318	−0.0343	−0.0398	−0.0507
$\hat{C}_4(T)$	−0.1436	−0.1657	−0.1854	−0.2041	−0.2443	−0.2738	−0.3235	−0.3292	−0.3197	−0.3155	−0.2958	−0.2805	−0.2589
$\hat{C}_5(T)$	0.0535	0.0500	0.0455	0.0401	0.0246	0.0092	−0.0354	−0.0601	−0.0794	−0.0833	−0.0938	−0.0976	−0.1000
$\hat{C}_6^0(T)$	−0.0174	−0.0120	−0.0133	−0.0189	−0.0393	−0.0585	−0.1003	−0.1142	−0.1198	−0.1200	−0.1167	−0.1110	−0.1004
$\hat{C}_6^1(T)$	−0.0030	0.0187	0.0313	0.0377	0.0382	0.0292	−0.0076	−0.0251	−0.0382	−0.0416	−0.0582	−0.0745	−0.1019
$\hat{C}_6^2(T)$	0.0365	0.0366	0.0390	0.0425	0.0508	0.0555	0.0528	0.0439	0.0341	0.0317	0.0224	0.0154	0.0046
Statistical Parameters for Distribution of Residuals for Northeast India													
$\hat{\alpha}(T)$	1.4706	1.3972	1.3512	1.3200	1.2742	1.2489	1.1970	1.1591	1.1064	1.0897	1.0143	0.9524	0.9312
$\hat{\beta}(T)$	0.9285	0.9495	0.9580	0.9598	0.9543	0.9476	0.9402	0.9470	0.9626	0.9680	0.9936	1.0144	0.9613
$N(T)$	10	10	10	10	10	10	10	10	10	10	10	10	8
Statistical Parameters for Distribution of Residuals for Western Himalaya													
$\hat{\alpha}(T)$	1.2821	1.3191	1.3341	1.3352	1.3146	1.2893	1.2364	1.2261	1.2323	1.2362	1.2579	1.2780	1.4103
$\hat{\beta}(T)$	0.9776	0.9583	0.9455	0.9376	0.9309	0.9331	0.9509	0.9602	0.9667	0.9681	0.9738	0.9786	0.9000
$N(T)$	10	10	10	10	10	10	10	10	10	10	10	10	8

of the residues at all the periods T for any desired probability p. The pseudo relative spectrum $PSV(T)$ with this probability of not being exceeded is then given by

$$\log_{10} PSV(T) = \log_{10} \hat{PSV}(T) + \in_p(T). \tag{14}$$

The distribution of Eq. (11) can also be used to estimate the probability of exceeding any specified spectral amplitude $PSV(T)$ due to the given values of governing parameters M,Δ, v, s, and s_L by estimating the corresponding residue $\in(T)$ from Eq. (10) using the least-squares estimate $\hat{PSV}(T)$ from Eq. (8a) or (8b). Such probabilities for different values of $PSV(T)$ are required in probabilistic seismic hazard computations [23,26,27,54,60,61,65–68].

4. Examples of estimated PSV spectra

Examples of estimated pseudo-relative velocity spectra (PSV) for damping $\zeta = 0.05$ are presented to illustrate that the proposed scaling relationships show a realistic dependence on all the parameters; viz., earthquake magnitude, epicentral distance, local geology, and site soil condition. Examples of the comparison of the estimated spectra with the spectra of actual accelerograms are also presented to show a direct test of the nature and reliability of the scaling relations developed.

4.1. Illustration of magnitude dependence

Fig. 12(a) and (b) show two sets of estimated PSV spectra to illustrate the dependence on earthquake magnitude. The results on the left-side plot are computed for the site geology parameter $s = 0$ (sediments) and $s = 2$ (basement rock) with soil parameter $s_L = 1$ (stiff soil), while those on the right-side plot are computed for soil parameter $s_L = 0$ (rock) and $s_L = 2$ (deep soil) with site geology parameter $s = 2$ (basement rock). To illustrate the typical dependence of the PSV amplitudes on magnitude, example results are computed for northeastern India only for $M = 3.5$, 4.5, 5.5, 6.5, and 7.5 at epicentral distance $R =$

Table 4.5
Smoothed Regression Coefficients and Statistical Parameters of Residues for the Scaling Models of Eqs. (8a) and (8b).

T (s)	0.04	0.06	0.08	0.10	0.15	0.20	0.40	0.60	0.80	1.0	1.5	2.0	3.0
Regression Coefficients for Scaling of PSV With $\zeta = 0.20$													
$\hat{C}_1^E(T)$	−2.1782	−2.0991	−2.1069	−2.1683	−2.3921	−2.5985	−3.0612	−3.3150	−3.6593	−3.7751	−4.3433	−4.8554	−5.6686
$\hat{C}_1^W(T)$	−2.2594	−2.1257	−2.0990	−2.1376	−2.3303	−2.5216	−2.9561	−3.1896	−3.5062	−3.6135	−4.1434	−4.6239	−5.3887
$\hat{C}_2(T)$	0.1575	0.0796	0.0446	0.0343	0.0457	0.0610	0.0503	0.0218	0.0222	0.0320	0.1154	0.2156	0.3914
$\hat{C}_3(T)$	−0.0680	−0.0605	−0.0566	−0.0547	−0.0527	−0.0509	−0.0400	−0.0311	−0.0251	−0.0245	−0.0269	−0.0327	−0.0442
$\hat{C}_4(T)$	−0.1663	−0.1896	−0.2090	−0.2264	−0.2621	−0.2877	−0.3311	−0.3372	−0.3306	−0.3275	−0.3125	−0.3009	−0.2845
$\hat{C}_5(T)$	0.0516	0.0471	0.0422	0.0368	0.0221	0.0080	−0.0330	−0.0560	−0.0744	−0.0782	−0.0887	−0.0929	−0.0959
$\hat{C}_6^0(T)$	−0.0361	−0.0360	−0.0395	−0.0457	−0.0637	−0.0793	−0.1102	−0.1186	−0.1199	−0.1193	−0.1134	−0.1065	−0.0948
$\hat{C}_6^1(T)$	0.0024	0.0148	0.0214	0.0239	0.0203	0.0114	−0.0181	−0.0306	−0.0398	−0.0424	−0.0562	−0.0704	−0.0950
$\hat{C}_6^2(T)$	0.0406	0.0353	0.0336	0.0342	0.0383	0.0415	0.0419	0.0374	0.0318	0.0303	0.0245	0.0197	0.0123
Statistical Parameters for Distribution of Residuals for Northeast India													
$\hat{\alpha}(T)$	1.4727	1.4073	1.3641	1.3336	1.2862	1.2586	1.2023	1.1639	1.1114	1.0947	1.0185	0.9560	0.9349
$\hat{\beta}(T)$	0.9448	0.9628	0.9694	0.9698	0.9622	0.9541	0.9453	0.9525	0.9691	0.9750	1.0025	1.0251	0.9756
$N(T)$	10	10	10	10	10	10	10	10	10	10	10	10	8
Statistical Parameters for Distribution of Residuals for Western Himalaya													
$\hat{\alpha}(T)$	1.2714	1.3182	1.3407	1.3473	1.3335	1.3093	1.2487	1.2320	1.2341	1.2377	1.2613	1.2856	1.4276
$\hat{\beta}(T)$	0.9745	0.9554	0.9432	0.9361	0.9309	0.9333	0.9480	0.9549	0.9599	0.9611	0.9667	0.9715	0.8928
$N(T)$	10	10	10	10	10	10	10	10	10	10	10	10	8

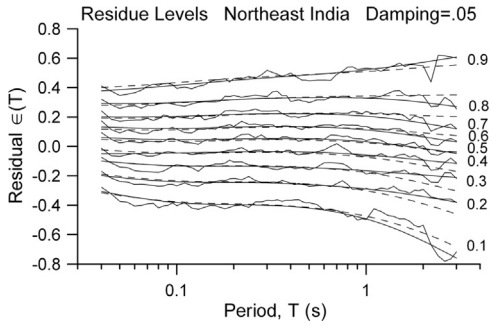

Fig. 8. The pseudo spectral velocity residues for $\zeta = 0.05$ and the approximation by Eq. (11) for probability levels of 0.1 through 0.9 for northeast India.

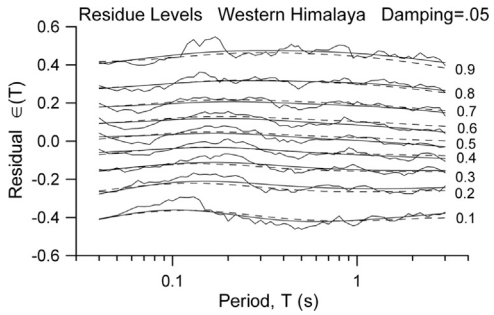

Fig. 9. The pseudo spectral velocity residues for $\zeta = 0.05$ and the approximation by Eq. (11) for probability levels of 0.1 through 0.9 for western Himalaya.

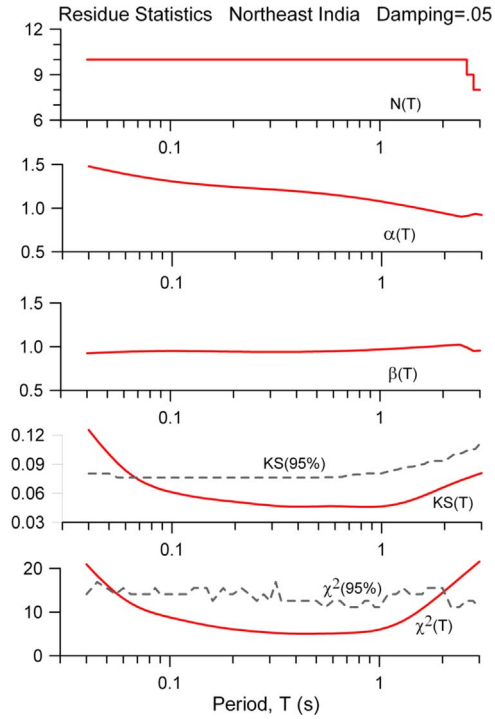

Fig. 10. Typical residue statistics of *PSV* spectrum amplitudes for $\zeta = 0.05$ in northeastern India.

0, focal depth $H = 10$ km, horizontal component of motion ($v = 0$), and for $p = 0.5$.

The growth rate of *PSV* amplitudes at high frequencies is seen to decrease with an increase in magnitude M, thus accounting for the magnitude-saturation effect in a physically realistic way. In Fig. 12(a), the effect of site geology is to amplify the *PSV* amplitudes on sediments compared to those on basement rock for periods longer than about 0.24 s, whereas the trend is reversed for short periods. On the other hand, the effect of site soil condition in Fig. 12(b) is to amplify the *PSV* amplitudes on deep soil sites for the entire period range, but the amplification diminishes with a decrease in the period.

4.2. Illustration of distance dependence

Fig. 13(a) and (b) show another two sets of curves of estimated *PSV* spectra for damping $\zeta = 0.05$ to illustrate the dependence on epicentral distance R in northeast India and western Himalaya, respectively. For the sole purpose of illustration, the examples are computed for $R = 0$, 25, 50, 100, and 200 km, magnitude $M = 6.5$, focal depth $H = 10$ km, local geology parameter $s = 1$ (intermediate sites), site soil parameter $s_L = 1$ (stiff soil), for $p = 0.5$ for horizontal ($v = 0$), as well as for vertical ($v = 1$) motions. The rate of decrease in *PSV* amplitudes with increase in distance is seen to slow down with an increase in the period, indicating expected slower attenuation of long period waves. Also, the

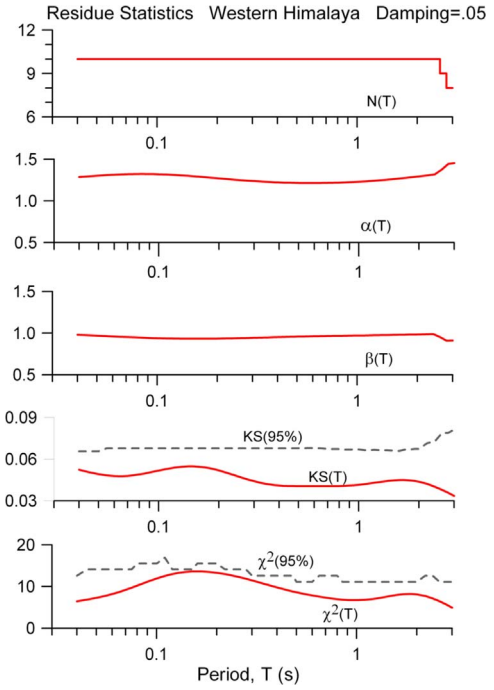

Fig. 11. Typical residue statistics of *PSV* spectrum amplitudes for $\zeta = 0.05$ in western Himalaya.

northeast Indian region is characterized by a significantly slower distance attenuation compared to the western Himalayan region. As the distance dependence is common for horizontal and vertical components of motion, spectral amplitudes at each period decrease by the same amount with an increase in distance for both $v = 0$ and 1. The horizontal *PSV* amplitudes are higher than the vertical amplitudes for the entire period range, but the gap decreases with a decrease in the period. This dependence is different from that of the Fourier spectrum amplitudes [38], which were seen to be higher for the vertical component of motion up to periods of about 0.09 s. This is because the response spectrum at low periods also has significant contributions from ground motion at longer periods.

4.3. Dependence on local geological and site soil conditions

Example results are next presented to illustrate the effects of local geological and site soil conditions on the estimated *PSV* amplitudes. As these effects are common to the regions of northeast India and western Himalaya, typical results for only western Himalaya for magnitude $M = 6.5$, distance $R = 25$ km, depth $H = 10$ km, and for horizontal ($v = 0$) component of motion are considered sufficient to demonstrate all major features of these effects. The three sets of plots in Fig. 14 show the typical variations in the *PSV* amplitudes for $\zeta = 0.05$ with site geological condition for three local site soil conditions defined by parameter $s_L = 0$ (rock), 1 (stiff soil), and 2 (deep soil). Three *PSV* spectra in each of these plots correspond to three different site geological conditions defined by parameter $s = 0$ (sediments), 1 (intermediate sites), and 2 (geological basement rock). It may be seen that for periods up to about 0.24 s, the spectral amplitudes for sediments are the lowest for all three site soil conditions. The trend is seen to be reversed for longer periods, with the spectral amplitudes on sediments attaining the highest values. However, the amplification effect at longer periods is more significant than the deamplification effect at shorter periods. This is because the lower periods (higher frequencies) have lower dynamic amplification with an increasing thickness of sediments due to anelastic attenuation. These trends are physically realistic and similar to those observed by [89,90] in California, and by Lee and Trifunac [56] in the former Yugoslavia.

The three sets of plots in Fig. 15 show the typical variations in the *PSV* amplitudes for $\zeta = 0.05$ with site soil conditions for three geologic site conditions defined by parameter $s = 0$ (sediments), 1 (intermediate sites), and 2 (geological basement rock). Three *PSV* spectra in each of these plots correspond to three different local site soil conditions defined by parameters $s_L = 0$ (rock), 1 (stiff soil), and 2 (deep soil). The *PSV* amplitudes are seen to increase from rock soil ($s_L = 0$), to stiff soil ($s_L = 1$), to deep soil ($s_L = 2$) at all the periods, but the amplification is not significant for periods shorter than about 0.1 s. This is because with increasing thickness and/or softness of soil, the shorter periods (higher frequencies) also experience more pronounced anelastic attenuation effect. The amplification trends in Fig. 15 are physically realistic and are similar to those observed by Trifunac [89] for California, and by Lee and Trifunac [56] in the former Yugoslavia.

4.4. Comparison with PSV spectra of actual accelerograms

Having shown that the estimated *PSV* spectra for northeast India and western Himalaya have a physically realistic dependence on magnitude M, source-to-site distance Δ, site geological parameter s, local soil parameter s_L, and the component of motion parameter v, the next test of our scaling relations is to compare the estimated spectra with those of actual accelerograms. Two typical examples of such comparisons are presented in Fig. 16(a) and (b), showing the actual spectra for five ratios of critical damping $\zeta = 0.00$, 0.02, 0.05, 0.10, and 0.20 by irregular solid curves and the corresponding estimated spectra for

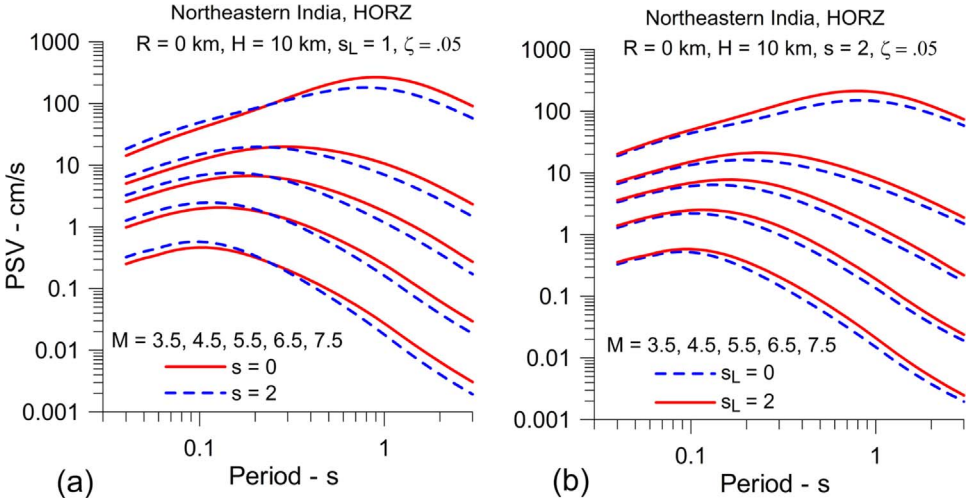

Fig. 12. Variations in the estimated *PSV* spectra of horizontal motion ($v = 0$) for $\zeta = 0.05$ in northeast India with magnitude for epicentral distance $R = 0$ km, focal depth $H = 10$ km, $p = 0.5$, and for (a) stiff soil ($s_L = 1$) type of site classification with local geology as sediments ($s = 0$) and basement rock ($s = 2$), and for (b) basement rock type of local geology ($s = 2$) with site classification as rock ($s_L = 0$) and deep soil ($s_L = 2$).

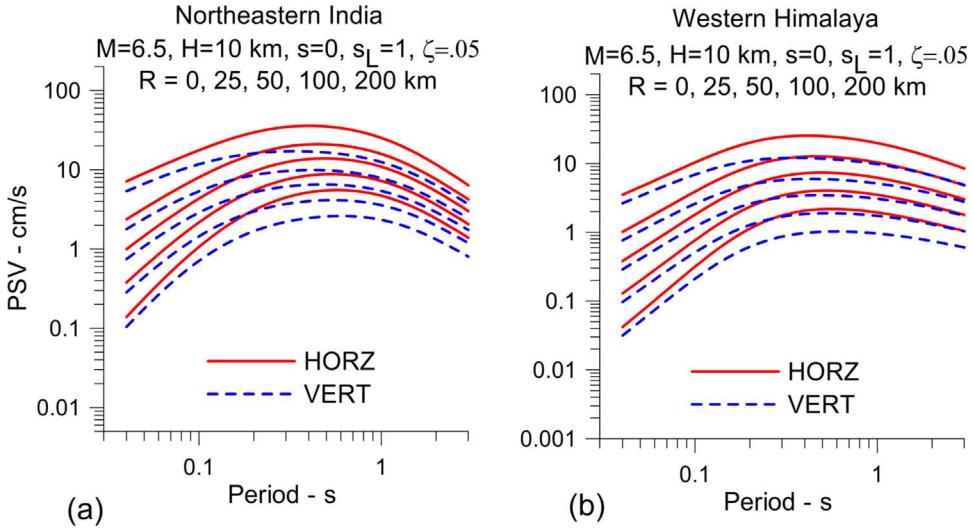

Fig. 13. Variations in the estimated *PSV* spectra of horizontal ($v = 0$) and vertical ($v = 1$) motions for $\zeta = 0.05$ with epicentral distance for magnitude $M = 6.5$, focal depth $H = 10$ km, site geology parameter $s = 1$ (intermediate sites), site soil classification $s_L = 1$ (stiff soil), and $p = 0.5$ for (a) northeast India and, (b) western Himalaya.

confidence levels of $p = 0.1$ and 0.9 by smooth dashed curves and smooth solid curves, respectively. The left side and middle plots represent the two horizontal components and the right-side plot is for the vertical motion component. The first line of the title at the top of both figures identifies the earthquake and record numbers, region, name and date of the earthquake, and the name of the recording site. The second line of the title gives the governing parameters of the record that are also used to compute the empirical $PSV(T)$ amplitudes. Results in Fig. 16(a) and (b) show good agreement between the actual and the estimated *PSV* spectra. The actual spectra are seen to mostly lie between the predicted spectra for $p = 0.1$ and 0.9, representing an 80% confidence interval.

5. Long- and short-period extensions of empirical PSV spectra

To extend the empirical *PSV* amplitudes outside the limited period range of their applicability, simple methods proposed by Trifunac [97,98] have been used. These methods of extrapolation have been recently used by Lee et al. [64–68] for *PSV* spectra in Serbia from the Vrancea earthquakes.

5.1. Long-period extension

Trifunac [97] proposed a method for long-period extension of *PSV* spectra by computing the displacement response spectra for the ground accelerations corresponding to Brune's [11] near- and far-field displacement pulses. The extension is achieved by matching the *PSV* spectra with the empirical spectra at the upper cut-off period T_C that is selected to eliminate inclusion in the empirical amplitudes of higher noise-to-signal ratios.

Normalizing the Brune near- and far-field displacements to amplitudes of unity, and considering only their time-dependent terms, their displacements are defined by $d_N(t) = (1 - e^{-t/\tau})$ and $d_F(t) = te^{-\alpha t}$, respectively. The relative displacement response of a single-degree-of-freedom (SDOF) oscillator with a natural frequency $\omega = 2\pi/T$ and damping ratio ζ to the ground accelerations associated with the far-field pulse is thus governed by the equation

$$\ddot{x}_r(t) + 2\omega\zeta\dot{x}_r(t) + \omega^2 x_r(t) = -\ddot{d}_F(t) = -(\alpha^2 t - 2\alpha)e^{-\alpha t}. \tag{15}$$

Similarly, the response to the near-field displacement is governed by

$$\ddot{x}_r(t) + 2\omega\zeta\dot{x}_r(t) + \omega^2 x_r(t) = -\ddot{d}_N(t) = -\frac{1}{\tau^2}e^{-t/\tau}. \tag{16}$$

With zero initial displacement and velocity response, the solution of Eq. (15) is given [97] as

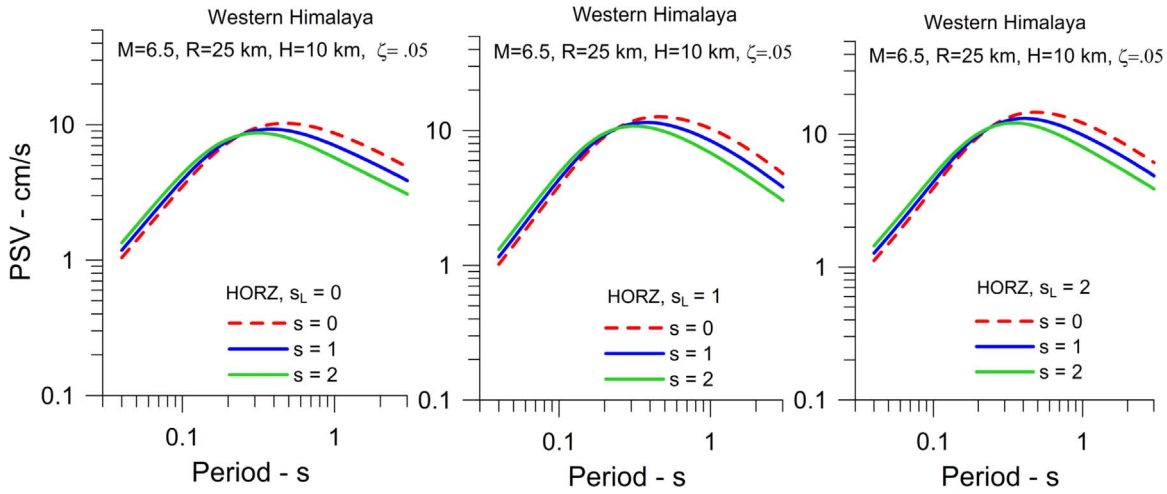

Fig. 14. The variations in the estimated *PSV* spectra of horizontal ($v = 0$) motion for $\zeta = 0.05$ with varying local geologic site condition from sediments ($s = 0$), to intermediate sites ($s = 1$), and to basement rock ($s = 2$) for western Himalaya. The left, middle, and right plots correspond to rock ($s_L = 0$), stiff soil ($s_L = 1$), and deep soil ($s_L = 2$) types of site soil classifications, respectively.

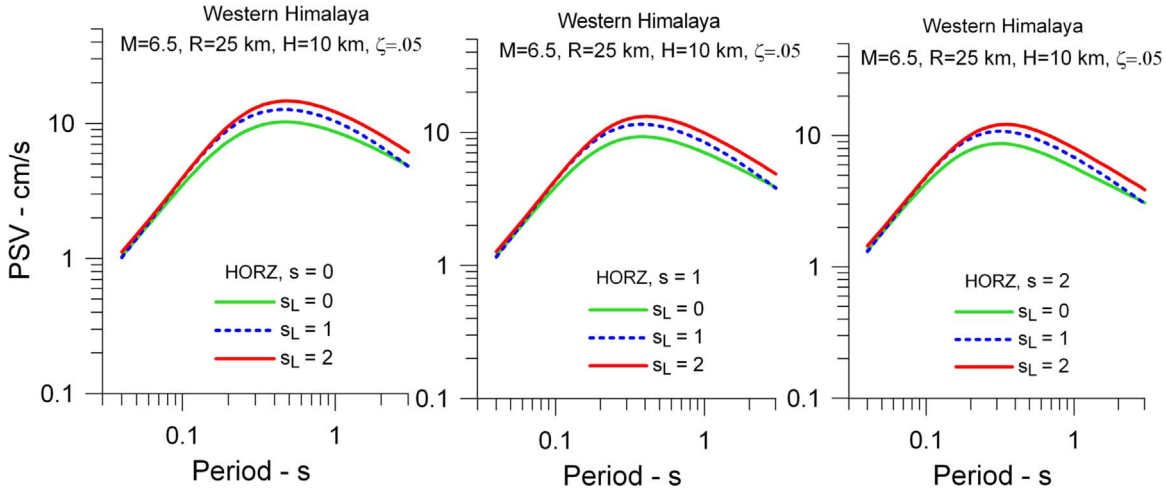

Fig. 15. The variations in the estimated *PSV* spectra of horizontal ($v = 0$) motion for $\zeta = 0.05$ with varying site soil conditions from rock ($s_L = 0$), to stiff soil ($s_L = 1$), to deep soil ($s_L = 2$), for western Himalaya. The left, middle, and right plots represent sites on sediments ($s = 0$), intermediate sites ($s = 1$), and basement rock ($s = 2$) geologic site conditions, respectively.

$$x_r(t) = e^{-\omega\zeta t}(a \sin \omega t + b \cos \omega t) + (A + Bt)e^{-\alpha t}, \tag{17}$$

with

$$B = \frac{-\alpha^2}{\alpha^2 - 2\omega\zeta\alpha + \omega^2}; \quad A = \frac{2\alpha - 2\omega\zeta B + 2\alpha B}{\alpha^2 - 2\omega\zeta\alpha + \omega^2}; \quad b = -A \quad \text{and} \quad a = \frac{\alpha A - B - 1 + b\omega\zeta}{\omega}. \tag{18}$$

The solution of Eq. (16) is also given in Trifunac [97] as

$$x_r(t) = e^{-\omega\zeta t}(a \sin \omega t + b \cos \omega t) + Ae^{-t/\tau}, \tag{19}$$

with

$$A = \frac{1}{1 + 2\zeta\omega\tau + (\omega\tau)^2}; \quad b = -A \quad \text{and} \quad a = \left(\frac{1}{\omega\tau} - \tau\right)A - \frac{1}{\omega\tau}. \tag{20}$$

Parameter α appearing in Eqs. (15), (17), and (18) represents the Brune [11] corner frequency defined by

$$\alpha = \frac{2.34\beta}{r} = \frac{2.34\beta}{W/2}. \tag{21}$$

Here, β is the shear-wave velocity at the source and r is the source dimension taken equal to one-half the fault rupture width W. The parameter τ in Eqs. (16), (19), and (20) is related to the displacement rise time, which can be approximated by [96] as

$$\tau \sim \frac{L}{v} + \frac{W}{2\beta}, \tag{22}$$

with L and W as the fault rupture length and rupture width, and v and β as the dislocation spreading velocity and the shear-wave velocity at the source, respectively. The dislocation spreading velocity can be approximated by 0.73 β. Following our recent study on the scaling of Fourier spectra for western Himalaya and northeast India [38], the rupture length L and width W for both regions can be approximated by

$$L = 0.0032 \times 10^{0.57M} \tag{23}$$

$$W = \begin{cases} 0.0278 \times 10^{0.41M} \text{for} M \geq 6.0 \\ L \text{for} M < 6.0 \end{cases}. \tag{24}$$

Also, as previously mentioned, the shear-wave velocity in the source region β is taken as 3.3 km/s and 3.5 km/s for western Himalaya and northeast India, respectively.

The absolute maximum values of the solutions in Eqs. (17) and (19) provide the shapes $X_F(T, \zeta)$ and $X_N(T, \zeta)$ of the relative displacement response spectra in the far- and near-fields, respectively. To compute these functions efficiently, Trifunac [97] provided empirical relationships to directly obtain the time, t_{max}/T, at which the absolute maxima occur. However, the solutions in Eqs. (17) and (19) are computed numerically at closely spaced time intervals to obtain their maximum amplitudes in the present study. If $PSV(T_C, \zeta)$ is the empirical spectral amplitude at the cut-off period T_C, the extended spectra $PSV_{FF}(T, \zeta)$ in the far-field beyond period T_C is obtained as [64–68,97]

$$PSV_{FF}(T, \zeta) = \frac{T_C PSV(T_C, \zeta)}{X_F(T_C, \zeta)} \cdot \frac{X_F(T, \zeta)}{T}. \tag{25}$$

Similarly, the extended spectra $PSV_{NF}(T, \zeta)$ in the near-field beyond period T_C is obtained using $X_N(T, \zeta)$ as

$$PSV_{NF}(T, \zeta) = \frac{T_C PSV(T_C, \zeta)}{X_N(T_C, \zeta)} \cdot \frac{X_N(T, \zeta)}{T}. \tag{26}$$

To have continuous transition from *NF* to *FF*, the spectrum beyond T_C is defined as a weighted combination of the spectra $PSV_{NF}(T, \zeta)$ and $PSV_{FF}(T, \zeta)$ as [97]

$$PSV(T, \zeta) = PSV_{NF}(T, \zeta)e^{-\left(\frac{3S_1}{4S}\right)} + PSV_{FF}(T, \zeta)\left(1 - e^{-\left(\frac{3S_1}{4S}\right)}\right), \tag{27}$$

with S_1 as the shortest distance between the site and the top of the fault, defined by

$$S_1 = \begin{cases} \sqrt{R^2 + (H - S)^2} & \text{for } H \geq S \\ R & \text{for } H < S \end{cases}, \tag{28}$$

where R is the epicentral distance and S is the dimension of the fault taken equal to length L obtained from Eq. (23) with an upper limit of 16.25 km corresponding to magnitude $M = 6.5$. The $PSV_{NF}(T, \zeta)$ defined by Eq. (26) is nearly constant for the period range of our empirical relations. Thus, to match the slope for the case of the near-field extension, period T_C in Eq. (26) is taken equal to the period of the peak amplitude of the empirical spectrum. For periods longer than the peak period, and up to the actual cutoff period used for the far-field extension, the empirical spectrum $PSV(T, \zeta)$ only is used in place of $PSV_{FF}(T, \zeta)$ in Eq. (27).

Fig. 17 (a) and (b) show the *PSV* spectra with $\zeta = 0.05$ thus extrapolated in the far field at $R = 300$ km using Eqs. (25)–(28) for northeast India and western Himalaya, respectively. The other parameters considered are: focal depth $H = 0$ km, local geology as basement rock ($s = 2$), site soil condition as rock soil ($s_L = 0$), and component of

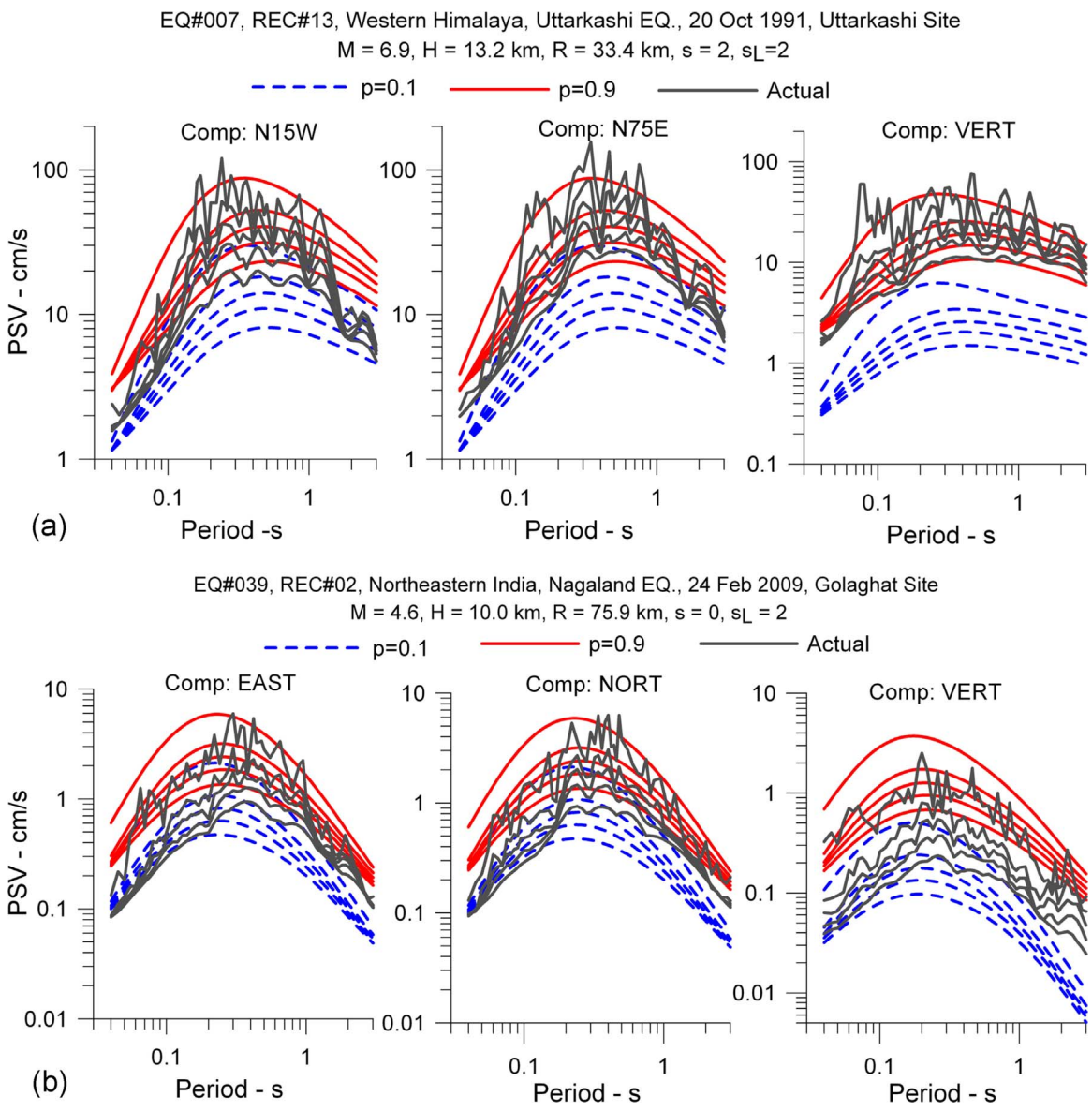

Fig. 16(. a). A comparison of the *PSV* spectra for $\zeta = 0.00$, 0.02, 0.05, 0.10, and 0.20 of recorded accelerograms for the October 20, 1991 Uttarkashi earthquake in western Himalaya at the Uttarkashi site with $M = 6.9$, $H = 13.2$ km, $R = 33.4$ km, $s = 2$, and $s_L = 2$, with the corresponding estimated response spectra. **(b)**. A comparison of the *PSV* spectra for $\zeta = 0.00$, 0.02, 0.05, 0.10, and 0.20 of recorded accelerograms for the February 24, 2009 Nagaland earthquake in northeast India at the Golaghat site with $M = 4.6$, $H = 10.0$ km, $R = 75.9$ km, $s = 0$, and $s_L = 2$, with the corresponding estimated response spectra.

motion as horizontal ($v = 0$). The cut-off periods of the empirical spectra for extrapolations in northeast India are taken as 0.3, 0.4, 0.7 s, and 1.0 s for magnitudes of 3.0, 4.0, 5.0, and greater than or equal to 6.0, respectively. For western Himalaya, these periods are taken as 0.4, 0.5, 1.0 s, and 1.5 s, respectively. Fig. 18 (a) and (b) show similar extrapolations for the relative velocity spectra in the near field at $R = 10$ km, with focal depth $H = 0$ km, basement rock type site geology ($s = 2$), and rock soil ($s_L = 0$) type of site condition. The cut-off periods for near-field extrapolations are taken as 0.15, 0.30, 1.0, 1.5, 3.0 s, and 1.0 s for $M = 3$, 4, 5, 6, 7, and 8 for both the northeast India and western Himalaya regions.

5.2. Short-period extension

The empirical scaling relations developed in this paper for *PSV* spectra are limited to a period of 0.04 s on the lower side. Trifunac [98] has proposed a method based on the random vibration theory to extend the relative velocity spectral amplitudes to periods below the lowest applicability period of the empirical relations. This method is based on computing the root mean square value of the response of an SDOF oscillator using empirical Fourier amplitude spectrum extended to lower periods (higher frequencies) and the transfer function of the oscillator. However, in the present work, a slightly modified method based on the power spectral density function (PSDF), $G(\omega)$, of ground acceleration is used, where $G(\omega)$ is obtained from the empirical relative velocity spectrum with zero damping and extended up to 0.01 s period, as described in Appendix A. This PSDF has been used to compute the expected amplitudes of relative displacement response spectrum also up to a period of 0.01 s using simple relationships from the random vibration theory.

In terms of $G(\omega)$, the PSDF of the relative displacement response, $r(t)$, of a SDOF oscillator with natural period T_j (frequency $\omega_j = 2\pi/T_j$) and damping ratio ζ can be written as

$$ED_j(\omega) = G(\omega)|H_j(\omega)|^2, \tag{29}$$

where $|H_j(\omega)|^2$ is the absolute squared transfer function of the SDOF

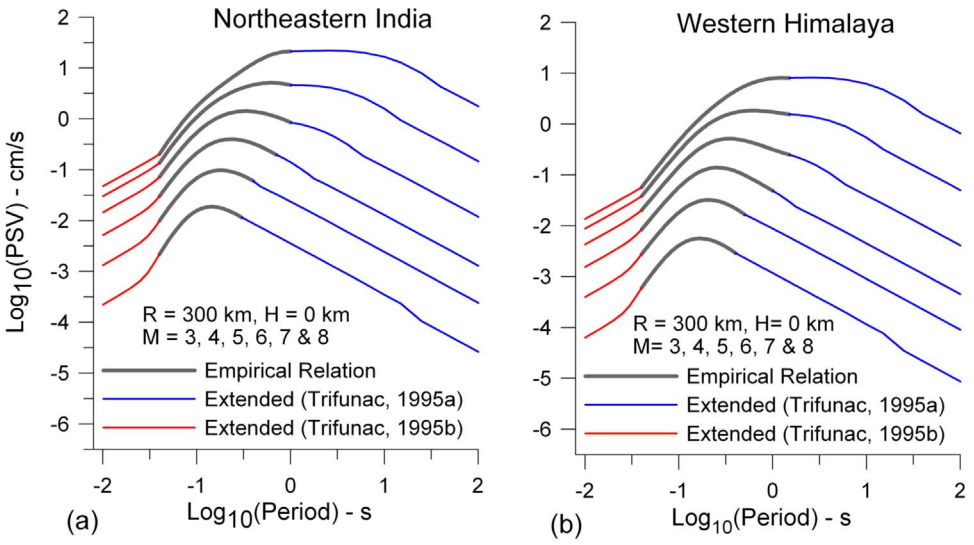

Fig. 17. Long- and short-period extensions of the horizontal components of empirical *PSV* spectra with $\zeta = 0.05$ in the far field for (a) northeast India and (b) western Himalaya for different magnitudes at epicentral distance $R = 300$ km, focal depth $H = 0$ km, local geology as basement rock ($s = 2$), soil site condition as "rock" ($s_L = 0$), and for $p = 0.5$.

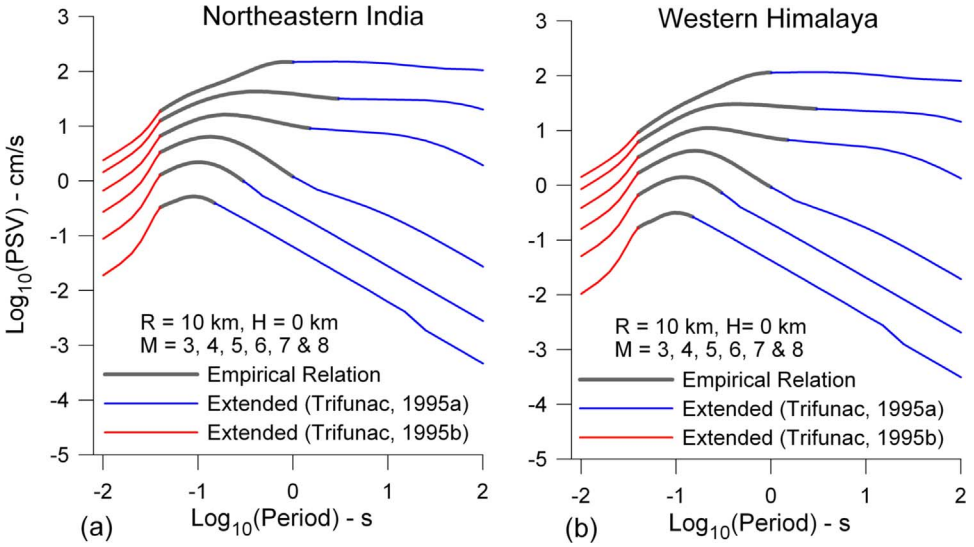

Fig. 18. Long- and short-period extensions of the horizontal component of empirical *PSV* spectra with $\zeta = 0.05$ in the near field for (a) northeast India and (b) western Himalaya for different magnitudes at epicentral distance $R = 10$ km, focal depth $H = 0$ km, local geology as basement rock ($s = 2$), soil site condition as "rock" ($s_L = 0$), and for $p = 0.5$.

oscillator defined by Eq. (A.3). The $ED_j(\omega)$ can be used to compute the expected displacement response spectrum for period T_j and damping ratio ζ from Eq. (A.4) as

$$\overline{SD}(T_j, \zeta) = r_{rms}[2 \ln (1 - \varepsilon^2)^{1/2} N]^{1/2}. \quad (30)$$

The parameters r_{rms}, ε, and N in this relationship are computed

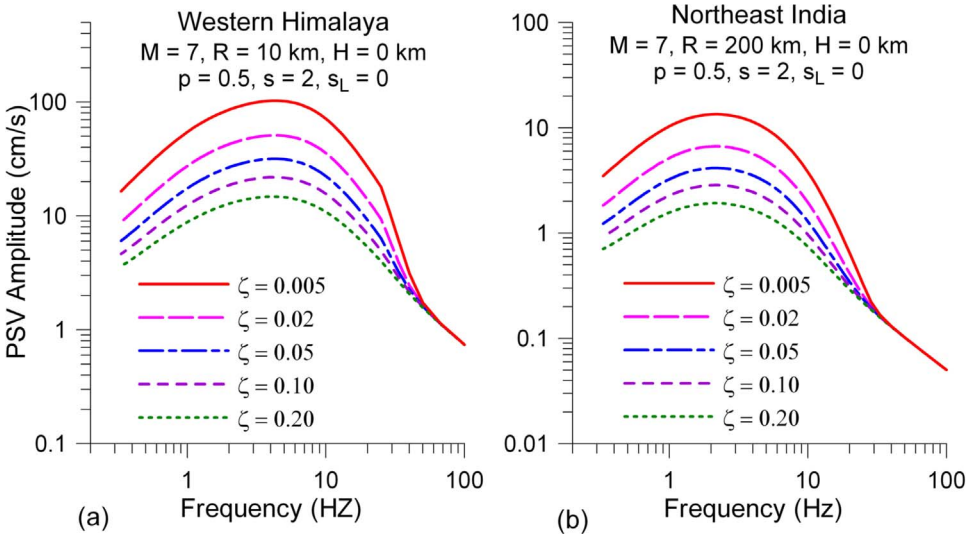

Fig. 19. Typical examples of the *PSV* spectra computed up to a frequency of 100 Hz (period of 0.01 s) for five damping ratios $\zeta = 0.00$, 0.02, 0.05, 0.10, and 0.20 using the PSDF of ground acceleration obtained from the empirical *PSV* spectrum with zero damping for (a) western Himalaya at R = 10 km and (b) northeast India at R = 200 km, computed for $M = 7$, $H = 0$ km, local geology as basement rock ($s = 2$), soil site condition as "rock" ($s_L = 0$), and for $p = 0.5$.

using the expressions of Eq. (A.5) in terms of the zeroth-, second-, and fourth-order moments m_0, m_2, and m_4 of $ED_j(\omega)$.

Fig. 19(a) and (b) shows typical examples of the PSV spectra corresponding to the $\overline{SD}(T, \zeta)$ spectra computed from Eq. (30) up to a natural frequency of 100 Hz (natural period 0.01 s) for five damping ratios of $\zeta = 0.005$, 0.02, 0.05, 0.10, and 0.20 for western Himalaya and northeast India, respectively. For the purpose of computation, the zero damping is represented by a nominal damping ratio of $\zeta = 0.005$, as discussed in Appendix A. The spectra in Fig. 19 are for a confidence level of $p = 0.5$, basement rock ($s = 2$) type of site geology, rock type of site soil ($s_L = 0$) condition, magnitude $M = 7$, focal depth $H = 0$ km, and epicentral distance $R = 10$ km for western Himalaya and 200 km for northeast India, respectively. The spectral amplitudes for all the damping ratios are seen to merge toward an asymptote with a -1 slope beyond certain frequency, which is seen to be higher for smaller distances. This is because the kappa factor responsible for the decay of high-frequency ground motion amplitudes increases with distance [38], causing faster decay at longer distances. For the frequency range over which the *PSV* amplitudes for different damping values coalesce, the corresponding PSA spectral amplitudes will attain a constant value that can be taken to represent the absolute peak ground acceleration $a_{\max}$.

The expected relative displacement spectrum amplitudes $\overline{SD}(T, \zeta)$ computed from Eq. (30) can be used to extend the empirical relative velocity spectrum $PSV(T, \zeta)$ at periods lower than the period T_L up to which the empirical relations are applicable, using

$$PSV(T, \zeta) = \frac{T_L PSV(T_L, \zeta)}{\overline{SD}(T_L, \zeta)} \cdot \frac{\overline{SD}(T, \zeta)}{T}; \quad T \le T_L. \tag{31}$$

The *PSV* spectral amplitudes extrapolated for periods below 0.04 s using Eq. (31) are also shown in Figs. 17 and 18.

5.3. Validation of the PSV extensions

Trifunac [97] has shown that the peak ground displacement, $d_{F,\max}$, in the far field can be related to the empirical relative velocity spectral amplitude, $PSV(T_C, \zeta)$, at the upper cut-off period, T_C, of applicability and the far-field relative displacement spectral amplitude, $X_F(T_C, \zeta)$, based on Brune's displacement pulse as follows:

$$d_{F,\max} = \frac{T_C}{2\pi\alpha e} \cdot \frac{PSV(T_C, \zeta)}{X_F(T_C, \zeta)}, \tag{32}$$

where α is the corner frequency and e is the base to the natural logarithm. The $PSV(T_C, \zeta)$ in Eq. (32) is computed for the desired earthquake magnitude, source-to-site distance, and site geology and site soil conditions parameters. The $d_{F,\max}$ in Eq. (32) is equivalent to the displacement response spectrum amplitude corresponding to the extended *PSV* spectrum at very long period $T \to \infty$. Thus, one possible way to test the validity of the long-period extension of relative velocity spectra is to compare the estimates of peak ground displacement computed from Eq. (32) with the values obtained by integration of the recorded accelerograms.

Fig. 20(a), (b) and (c) present the plots of such comparisons for the recorded data in the epicentral distance range of 100(± 25) km for northeast India and ranges of 20(± 5) km and 100(± 25) km for western Himalaya. The peak displacement values from the recorded accelerograms used for comparison in Fig. 20 have been also scaled to compensate approximately for the effects of high-pass filtering applied during baseline correction, using a method due to [62], based on the empirical Fourier amplitude spectra extended up to a 100 s period from Gupta and Trifunac [38]. The $d_{F,\max}$ values in each of the plots of Fig. 20 are estimated for the central value of each distance range, and for magnitudes of 3.0–8.0, basement rock ($s = 2$) type of site geology, rock type of site soil ($s_L = 0$) condition, and for $p = 0.1$, 0.5 and 0.9. The solid curve in each plot represents $d_{F,\max}$ for $p = 0.5$ and two dashed curves for $p = 0.1$ and 0.9. It is seen that the peak displacement

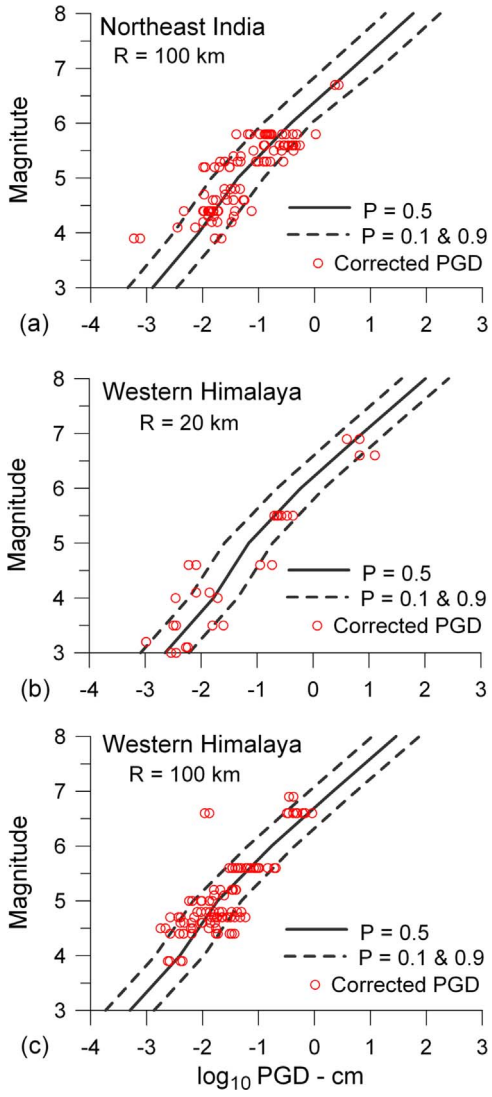

Fig. 20. Comparisons of the corrected peak ground displacements in the recorded data (open circles) in the epicentral distance range of 100(± 25) km for northeast India and ranges of 20(± 5) km and 100(± 25) km for western Himalaya, with $d_{F,\max}$ values estimated for the central value of each distance range, and for magnitudes of 3.0–8.0, basement rock ($s = 2$) type of site geology, rock type of site soil ($s_L = 0$) condition, and for $p = 0.1$, 0.5 and 0.9. The solid curve in each plot represents $d_{F,\max}$ for $p = 0.5$ and two dashed curves for $p = 0.1$ and 0.9.

estimates based on extended empirical *PSV* spectrum amplitudes are in very good agreement and consistent with the independent estimates from the recorded accelerograms.

Using the expression for the zero frequency far-field source spectrum of Keilis-Borok [46], Trifunac [97] has also shown that the peak displacement $d_{F,\max}$ defined by Eq. (32) can be related to the seismic moment M_0 as

$$M_0 = 4\pi\mu_{source}\beta_{source}R\alpha e d_{F,\max}/\alpha^2, \tag{33}$$

where μ_{source} and β_{source} are the shear modulus and shear wave velocity in the earthquake source region and R is the epicentral distance. As in Gupta and Trifunac [38], the values of μ_{source} for northeast India and western Himalaya are taken to be 3.4×10^{11} dyne/cm^2 and 3.0×10^{11} dyne/cm^2, respectively. Also, as previously mentioned, the values of β_{source} for the two regions are taken as 3.5 km/s and 3.3 km/s, respectively. The validity of the long-period extension of *PSV* spectra in the far field has been tested further by comparing the seismic moment estimates from Eq. (33) with other independent seismological estimates for northeast India and western Himalaya in Fig. 21 (a) and (b),

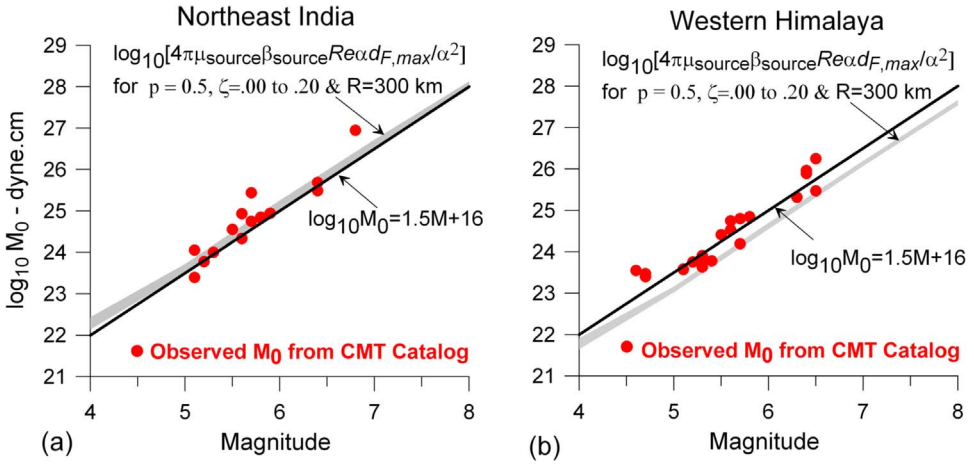

Fig. 21. A comparison of seismic moment estimates from Eq. (33) with the empirical line and values from the CMT catalog for (a) northeast Indian and (b) western Himalayan earthquakes.

respectively.

The values of M_0 in Fig. 21 are computed using the $d_{F,\max}$ for values of magnitude $M = 4, 5, 6, 7$, and 8 for damping ratios $\zeta = 0.00$–0.20, and for distance $R = 300$ km, site geology as basement rock ($s = 2$), site soil condition as rock type ($s_L = 0$), and for $p = 0.5$. The $\log_{10}M_0$ values computed from Eq. (33) are compared with the seismological values available from the CMT catalog (www.globalcmt.org) for many of the earthquakes contributing to the strong-motion database used in this study and with the empirical relationship $\log_{10}M_0 = 1.5M + 16$ [43]. The agreement of the estimated $\log_{10}M_0$ values with the observed values from the CMT catalog, as well as with the empirical line for the northeastern India, is seen to be good. The estimated values for western Himalaya are seen to be lower than the observed values as well as the empirical line. However, the deviations are small, and can be attributed to faster attenuation with distance in the western Himalayan region. Similar observations were made for western Himalaya in our paper on the scaling of Fourier amplitude spectra [38]. Thus, the M_0 estimates can be also considered to be consistent with the other independent estimates vis-à-vis the long-period extension of empirical *PSV* spectra for western Himalaya.

Finally, to test the validity of short-period (high-frequency) extension of *PSV* amplitudes, the pseudo spectral acceleration amplitudes at very short periods are approximated to represent the peak ground acceleration $a_{\max}$. The $a_{\max}$ values thus estimated using the extended *PSV* amplitudes at a 0.01 s period (100 Hz frequency) are compared with the peak ground acceleration values from the recorded accelerograms for the northeast India and western Himalaya regions in Fig. 22 (a), (b), and (c). Fig. 20 (a) presents the comparison plots for northeast India for recorded data in the epicentral distance range of 100(± 25) km, and Fig. 22(b) and (c) for western Himalaya for distance ranges of 20(± 5) km and 100(± 25) km, respectively. The $a_{\max}$ values in each of these plots are estimated for the central value of each distance range and for magnitudes of 3.0–8.0, basement rock ($s = 2$) type of site geology, rock type of site soil ($s_L = 0$) condition, and for $p = 0.1$, 0.5, and 0.9. The solid curve in each plot represents $a_{\max}$ for $p = 0.5$ and two dashed curves for $p = 0.1$ and 0.9. The peak acceleration estimates based on the short-period extension of empirical *PSV* spectrum amplitudes are seen to be in very good agreement and consistent with independent estimates from the recorded accelerograms.

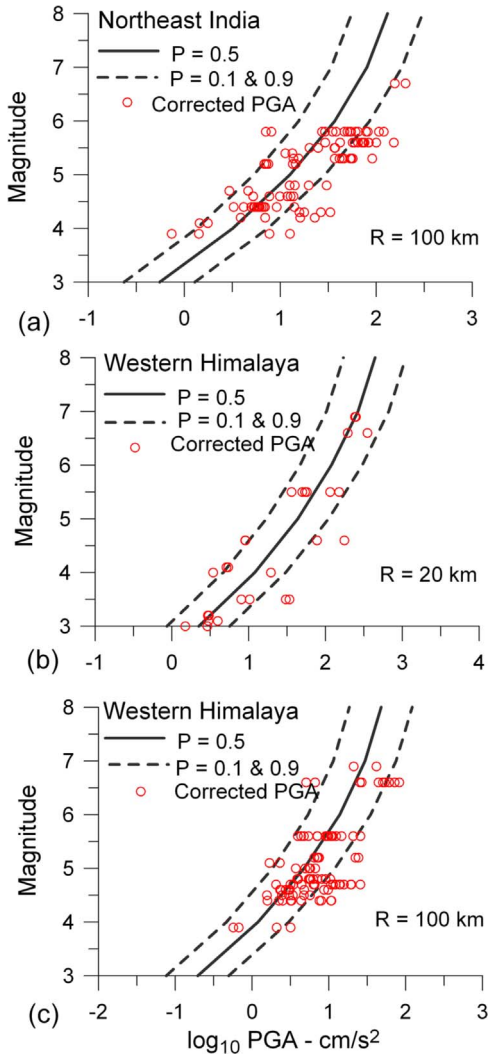

Fig. 22. Comparisons of the corrected peak ground acceleration in the recorded data (open circles) in the epicentral distance range of 100(± 25) km for northeast India and ranges of 20(± 5) km and 100(± 25) km for western Himalaya, with *PSA* values estimated for the central value of each distance range, and for magnitudes of 3.0–8.0, basement rock (= 2) type of site geology, rock type of site soil (=0) condition, and for = 0.1, 0.5 and 0.9. The solid curve in each plot is for p = 0.5 and two dashed curves for p = 0.1 and 0.9.

6. Discussion and conclusions

In this paper, we developed empirical scaling relations for the *PSV* spectral amplitudes for five ratios of critical damping $\zeta = 0.00$, 0.02, 0.05, 0.10, and 0.20 using a database of 1095 components of strong-motion accelerograms recorded in the highly seismic regions of western Himalaya and northeastern India. The frequency-dependent attenuation functions developed for the Fourier spectrum amplitudes in the two regions in our previous work [38] are used to also describe the attenuation of *PSV* amplitudes. Further, similar to that of the Fourier

amplitudes, the dependence of *PSV* amplitudes on earthquake magnitude, site geology and soil conditions, and the component of motion is assumed to be common to both western Himalaya and northestern India. This assumption became necessary due to the limited number of available data for independent regression analyses for the two regions. Although there is no strong reason to believe that the *PSV* amplitudes in western Himalaya and northeast India should have significantly different dependence on local geology, site soil conditions, and components of motion, the dependence on magnitude may perhaps be different. To normalize for the effects of such a dependence to some extent, the constant term representing the relative source strength is estimated separately for the two regions in the second step of regression for magnitude dependence.

The proposed PSV scaling relations for western Himalaya and northeastern India are shown to constrain the magnitude and source-to-site dependences in a physically realistic manner, with the saturation effects accounted for as the magnitude increases to very large values and the distance becomes small. The effects of site geologic and soil conditions are also represented in a realistic manner. For a given site soil type, the *PSV* amplitudes are amplified on geological sediments (relative to basement rock) for periods longer than about 0.24 s and slightly deamplified for smaller periods. This behavior can be considered realistic, because the lower period ground motion amplitudes experience strong anelastic attenuation. However, the effect of the local soil is to amplify the *PSV* amplitudes at all the periods compared to the rock soil, but the amplification is only slight for periods shorter than about 0.1 s. This behavior is also physically realistic, because the anelastic attenuation of ground motion amplitudes at lower periods is smaller for thin soil layer, which is overcome in the response spectral amplitudes due to significant contributions from the ground motion amplitudes at longer periods.

To estimate the empirical response spectrum with any desired probability of not exceeding (confidence level), probability distributions are also developed for the residuals between the *PSV* amplitudes of the recorded accelerograms and the corresponding empirical estimates for each natural period. Following Trifunac and colleagues [110,112,49–51], the distribution function has been used to describe the *PSV* residuals in the present work. Because the residuals have to follow the same probability distribution as the response spectrum amplitudes, which represent the highest response amplitude of SDOF oscillators, their distribution is considered to be appropriate. The commonly used Gaussian distribution can be also considered appropriate for the parameters that directly define the ground motion amplitudes and was used in our recent study to describe the residuals of Fourier amplitudes [38]. Kolmogorov–Simirnov and Chi-square tests have been performed to support the suitability of the probability distributions proposed to describe the residuals of *PSV* amplitudes in the present study. A few examples of the comparisons between the PSV spectra of actual accelerograms with the empirical spectra computed for confidence levels of $p = 0.1$ and 0.9 show that the actual spectra mostly lie within the 10–90% confidence interval, and that the trends of the empirical spectra are in good agreement with the actual spectra. The probability distributions of the residuals can also be used to compute the probability of exceeding a given spectral amplitude, $PSV(T)$, due to specified values of earthquake magnitude, distance, and site condition parameters, which form an essential input to the probabilistic seismic hazard computations.

To minimize the effects of low- and high-frequency noise present in the recorded and digitized accelerograms, the present empirical relations are defined in a limited period range of 0.04–3.0 s. The actual usable period may be narrower still, depending on the earthquake magnitude and distance. For the periods longer and shorter than the applicable period range, it has been shown that the empirical spectra can be extended using the methods proposed by Trifunac [97,98]. The long-period extension is based on the ground motion excitations defined approximately by Brune's [11] near- and far-field displacements; whereas the short- period extension is based on the classical results of Rice [73,74] and Cartwright and Longuet-Higgins [12] to compute the expected value of the highest amplitude in a stationary stochastic time-history. Several tests have been performed to show that the present empirical scaling relations for *PSV* amplitudes and their short- and long-period extensions have excellent consistency and good agreement with the independent estimates of the peak ground acceleration and peak ground displacement amplitudes from recorded accelerograms at close distances, as well as with the estimates of the seismic moment from distant seismological recordings. Thus, the proposed scaling relations can be considered to provide an improved basis for realistic macro- and microzonations of western Himalaya and northeastern India in terms of the uniform hazard response spectrum amplitudes at different natural periods [26].

Appendix A

An iterative method is presented to obtain the power spectral density function (PSDF) of ground acceleration from the empirical *PSV* spectrum with zero damping and extending it up to a desired highest frequency of interest using the kappa attenuation of high-frequency Fourier spectrum amplitudes [6]. This method is a simplification of the method of Gupta and Trifunac [36] for estimating the response spectrum compatible PSDF of ground acceleration. To avoid numerical instabilities, the zero damping is approximated by a damping ratio of $\zeta = 0.005$ in the present computations.

Let $PSV(T_j)$ be the given empirical spectral amplitudes at discrete periods T_j (frequencies $\omega_j = 2\pi/T_j$) with a lower limit of T_L ($\omega_L = 2\pi/T_L$). The corresponding relative displacement spectral amplitudes can be then defined by

$$SD(T_j) = PSV(T_j) \times T_j/2\pi. \tag{A.1}$$

Representing the required PSDF of ground acceleration at the ith step of the iteration by $G_i(\omega)$, the PSDF of the relative displacement response, $r(t)$, of an SDOF oscillator with natural period T_j and damping ratio $\zeta(=0.005)$ can be written as

$$ED_{ij}(\omega) = G_i(\omega)|H_j(\omega)|^2, \tag{A.2}$$

where $|H_j(\omega)|^2$ is the absolute squared transfer function of the SDOF oscillator

$$|H_j(\omega)|^2 = \frac{1}{(\omega_j^2 - \omega^2)^2 + (2\zeta\omega_j\omega)^2}. \tag{A.3}$$

The PSDF of Eq. (A.2) can be used to compute the expected maximum value $E[r_{\max}]$ of the SDOF response $r(t)$ using the classical work of Rice [73,74] and Cartwright and Longuet-Higgins [12] on the statistics of maxima in a stationary stochastic time history as follows:

$$E[r_{\max}] = r_{rms}\cdot[2\ln(1-\varepsilon^2)^{1/2}N]^{\frac{1}{2}}. \tag{A.4}$$

The various quantities in this expression are defined in terms of the zeroth-, second-, and fourth- order moments m_0, m_2 and m_4 of $ED_{ij}(\omega)$ as follows [12,36]:

$$r_{rms} = \sqrt{m_0},\ N = \frac{T_S}{\pi}\sqrt{\frac{m_4}{m_2}} \text{ and } \sqrt{1 - \frac{m_2^2}{m_0 m_4}}. \tag{A.5}$$

Here, T_S is the duration of $r(t)$, the choice of which is not very critical as long as it is long enough to satisfy the condition of stationarity of the response and the same value that is used in computing the spectral amplitudes is used in computing the PSDF of ground acceleration from the given PSV spectrum. A value of $T_S = 10$ s is considered appropriate for the present application.

The expected maximum response $E[r_{\max}]$ in Eq. (A.3) is by definition the expected relative displacement spectral amplitude $\overline{SD}(T_j)$, in terms of which the updated PSDF of ground acceleration for the next iteration is defined by

$$G_{i+1}(\omega) = \begin{cases} G_i(\omega) SD^2(T = \omega/2\pi)/\overline{SD}^2(T = \omega/2\pi); \text{ for} \omega \le \omega_{\mathrm{L}} \\ \mathrm{G_{i+1}}(\omega_L) e^{-(\omega-\omega_L)k}; \quad \text{for } \omega > \omega_L \end{cases}. \tag{A.6}$$

To start with the iterations, the initial PSDF of ground acceleration is defined in terms of the relative displacement spectrum from Eq. (A.1) as [36]

$$G_0(\omega) = \begin{cases} \frac{4\xi\omega^3}{\pi}\left[\frac{SD(T = 2\pi/\omega)}{2.0}\right]^2; \text{ for} \omega \le \omega_L \\ \mathrm{G_0}(\omega_L) e^{-(\omega-\omega_L)k}; \quad \text{for } \omega > \omega_L \end{cases}. \tag{A.7}$$

The high-frequency extensions of $G_0(\omega)$ and $G_{i+1}(\omega)$ in Eqs. (A.7) and (A.6) are based on the fact that the PSDF of ground acceleration is proportional to the square of the Fourier amplitude spectrum of ground acceleration, which decays at higher frequencies as $\exp(-\pi k f)$, with decay factor k (in s) [6]. The values of k for the basement rock type of site geology and rock type of site soil conditions ($s = 2$ and $s_L = 0$) used for computing the example results in the present study for western Himalaya and northeast India are obtained from the relations of Eqs. (29) and (30) in Gupta and Trifunac [38].

References

[1] Abrahamson NA, Silva WJ. Empirical response spectral attenuation relations for shallow crustal earthquakes. Seismol Res Lett 1997;68(1):94–127.
[2] Ambraseys NN, Douglas J, Sarma SK, Smit PM. Equations for the estimation of strong ground motions from shallow crustal earthquakes using data from Europe and the middle East: horizontal peak ground acceleration and spectral acceleration. Bull Earthq Eng 2005;3(1):1–53.
[3] Ambraseys NN, Douglas J, Sarma SK, Smit PM. Equations for the estimation of strong ground motions from shallow crustal earthquakes using data from Europe and the middle East: vertical peak ground acceleration and spectral acceleration. Bull Earthq Eng 2005;3(1):55–73.
[4] Amini A, Trifunac MD. Statistical extension of response spectrum superposition. Soil Dyn Earthq Eng 1985;4(2):54–63.
[5] Anagnostopoulos SA. Response spectrum techniques for three-component earthquake design. Earthq Eng Struct Dyn 1981;9:459–76.
[6] Anderson JG, Hough SE. A model for the shape of the Fourier amplitude spectrum of acceleration at high frequencies. Bull Seism Soc Am 1984;74:1969–94.
[7] Ashish C, Lindholm IA, Parvez, Kuhn D. Earthquake hazard assessment for Peninsular India. J Seismol 2016;20:629–53. http://dx.doi.org/10.1007/s10950-015-9548-2.
[8] Atkinson GM, Boore DM. Empirical ground-motion relations for subduction-zone earthquakes and their application to Cascadia and other regions. Bull Seism Soc Am 2003;93(4):1703–29.
[9] Biot MA. Theory of elastic systems vibrating under transient impulse with an application to earthquake-proof buildings. Proc Natl Acad Sci USA 1933;19(2):262–8.
[10] Biot MA. Analytical and experimental methods in engineering seismology. Proc ASCE 1942;68:49–69.
[11] Brune JN. Tectonic stress and the spectra of seismic shear waves. J Geophys Res 1970;75(26):4997–5009.
[12] Cartwright DE, Longuet-Higgins MS. The statistical distribution of maxima of a random function. Proc Roy Soc Lond Ser A 1956;327:212–32.
[13] Chandrasekaran AR. Strong motion arrays in India, in: Proceedings of the ninth world conference on earthquake engineering, VIII, 131–136; 1988.
[14] Chandrasekaran AR. Evaluation of design earthquake parameters for a site and utilization of strong motion data. Curr Sci 1994;67(5):353–8.
[15] Chandrasekaran AR, Das JD. Strong motion arrays in India and characteristics of recent recorded events. Bull Ind Soc Earthq Tech 1990;27(1):1–66.
[16] Chandrasekaran AR, Das JD. Strong motion arrays in India and analysis of data from Shillong array. Curr Sci 1992;62(1–2):233–50.
[17] Das S, Gupta ID, Gupta VK. A probabilistic seismic hazard analysis of northeast India. Earthq Spectra 2006;22(1):1–27.
[18] Das R, Sharma ML, Wason HR. Probabilistic seismic hazard assessment for northeast India. Pure Appl Geophys 2016. http://dx.doi.org/10.1007/s00024-016-1333-9.
[19] Dasgupta S, Pande P, Ganguly D, Iqbal Z, Sanyal K, Venkatraman NV, Dasgupta S, Sural B, Harendranath L, Mazumdar K, Sanyal S, Roy A, Das LK, Misra PS, Gupta H. Seismotectonic Atlas of India and its Environs. In: Narula PL, Acharyya SK, Banerjee J, editors. Geol. Surv. India Special Publ. No.59. 2000. p. 87.
[20] DerKiureghian A, Nakamura Y. CQC modal combination rule for high-frequency modes. Earthq Eng Struct Dyn 1993;22:943–56.
[21] Douglas J. Ground Motion Prediction Equations 1964–2016, Report, Department of Civil and Environmental Engineering, University of Stratchlyde, Glasgow, U.K (available online a; 2017. ⟨www.gmpe.org.wk/gmpereport2014.pdf⟩).
[22] Goodman LE, Rosenblueth E, Newmark NM. Aseismic design of firmly founded elastic structures. Trans ASCE 1958;120:782–802.
[23] Gupta ID. The state of the art in seismic hazard analysis. ISET Jour Earthq Tech 2002;39(4):311–46.
[24] Gupta ID. Defining source-to-site distances for evaluation of design earthquake ground motion, Proceedinds of the 13th symposium on earthquake engineering, IIT, Roorkee, 18-20 December 2006, Vol. I, pp. 295–306.
[25] Gupta ID. Delineation of probable seismic sources in India and neighborhood by a comprehensive analysis of seismotectonic characteristics of the region. Soil Dyn Earthq Eng 2006;26(8):766–90.
[26] Gupta ID. Probabilistic seismic hazard analysis method for mapping of spectral amplitudes and other design specific quantities to estimate the earthquake effects on manmade structures. ISET Jour Earthq Tech 2007;44(1):127–67.
[27] Gupta ID. Seismic hazard mapping methodologies, in: Proceedings of the international conference on earthquake engineering, Banja Luka, 26-28 October 2009, 55-101; 2009.
[28] Gupta ID. Response spectral attenuation relations for in-slab earthquakes in Indo-Burmese subduction zone. Soil Dyn Earthq Eng 2010;30:368–77.
[29] Gupta ID. Uniformly processed strong motion database for Himalaya and northeast region of India. Pure Appl Geophys 2017. [Accepted].
[30] Gupta ID, Joshi RG. An improved spectrum superposition method for structures with rigid modes. Nucl Eng Des 1998;185:293–307.
[31] Gupta ID, Joshi RG. Response spectrum superposition for structures with uncertain properties. J Eng Mech Div ASCE 2001;127(3):233–41.
[32] Gupta ID, Joshi SG. Response spectrum–based stochastic method for earthquake analysis of gravity dams. J Eng Mech Div ASCE 2017;143(5):1–14. http://dx.doi.org/10.1061/(ASCE)EM.1943-7889.0001171.
[33] Gupta ID, Trifunac MD. Order statistics of peaks in earthquake response of multi-degree-of-freedom systems. Earthq Eng Eng Vib 1987;7(4):15–50.
[34] Gupta ID, Trifunac MD. Probabilistic spectrum superposition for response analysis including the effects of soil-structure interaction. Probab Eng Mech 1990;5(1):9–18.
[35] Gupta ID, Trifunac MD. An improved probabilistic spectrum superposition. Soil Dyn Earthq Eng 1998;17:1–11.
[36] Gupta ID, Trifunac MD. Defining equivalent stationary PSDF to account for non-stationarity of earthquake ground motion. Soil Dyn Earthq Eng 1998;17:89–99.
[37] Gupta ID, Trifunac MD. Statistics of ordered peaks in the response of non-classically damped structures. Probab Eng Mech 1999;14:329–37.
[38] Gupta ID, Trifunac MD. Scaling of Fourier spectra of strong earthquake ground motion in western Himalaya and northeastern India. Soil Dyn Earthq Eng 2017;102:137–59. http://dx.doi.org/10.1016/j.soildyn.2017.08.010.
[39] Gupta VK, Trifunac MD. Response of multistoried buildings to ground translation and rocking during earthquakes. Probab Eng Mech 1990;5(3):138–45.
[40] Gupta VK, Trifunac MD. Response of multistoried buildings to ground translation and torsion during earthquakes. Eur Earthq Eng 1990;IV(1):34–42.
[41] Gupta VK, Trifunac MD. Seismic response of multistoried buildings including the effects of soil structure interaction. Soil Dyn Earthq Eng 1991;10(8):414–22.
[42] Gusev AA. Descriptive statistical model of earthquake source radiation and its application to an estimation of short-period strong motion. Geophys J R Astron Soc 1983;74(3):787–808.
[43] Hanks TC, Kanamori H. A moment magnitude scale. J Geophys Res 1979;84:2348–50.
[44] Johnson RA. An earthquake spectrum prediction technique. Bull Seism Soc Am 1973;63(4):1255–74.
[45] Joyner WB, Boore DM. Methods for regression analysis of strong-motion data. Bull Seism Soc Am 1993;83(2):469–87.
[46] Keilis-Borok VI. Investigation of the mechanism of earthquakes, Sov. Res. Geophys., 4 (Trans. Tr. Geofiz. Inst., 40), Am. Geophys. Union. NewYork:

Consultants Bureau; 1960.
[47] Kolathayar S, Sitharam TG. Comprehensive probabilistic seismic hazard analysis of the Andaman-Nicobar Regions. Bull Seism Soc Am 2012;102(5):2063–76.
[48] Kumar A, Mittal H, Sachdeva R, Kumar A. Indian strong motion instrumentation network. Seismol Res Lett 2012;83(1):59–66.
[49] Lee VW. Influence of local soil and geologic site conditions on pseudo relative velocity response spectrum amplitudes of recorded strong motion accelerations [Report CE 87-05]. Los Angeles, USA: University of Southern California; 1987.
[50] Lee VW. Empirical scaling of pseudo relative velocity spectra of recorded strong earthquake motion in terms of magnitude and both local soil and geologic site classifications. Earthq Eng Eng Vib 1989;9(3):9–29.
[51] Lee VW. Scaling PSV from earthquake magnitude, local soil, and geologic depth of sediments. J Geotech Eng, ASCE 1993;119(1):108–26.
[52] Lee VW. Pseudo relative velocity spectra in former Yogoslavia. Eur J Earthq Eng 1995;VII(1):12–22.
[53] Lee VW. Empirical scaling and regression methods for earthquake strong motion spectra—A review. ISET J Earthq Tech 2007;44(1):39–69.
[54] Lee VW, Trifunac MD. Uniform risk spectra of strong earthquake ground motion: NEQRISK [Report CE 85-05]. Los Angeles, USA: University of Southern California; 1985.
[55] Lee VW, Trifunac MD. Empirical models for scaling Fourier amplitude spectra of strong ground acceleration in terms of earthquake magnitude, source to station distance, site intensity and recording site conditions. Soil Dyn Earthq Eng 1989;8(3):110–25.
[56] Lee VW, Trifunac MD. Frequency dependent attenuation of strong earthquake ground motion in Yugoslavia. Eur Earthq Eng 1992;VI(1):3–13.
[57] Lee VW, Trifunac MD. Empirical scaling of Fourier amplitude spectra in former Yugoslavia. Eur Earthq Eng 1993;VII(2):47–61.
[58] Lee VW, Trifunac MD. Frequency dependent attenuation function and fourier amplitude spectra of strong earthquake ground motion in California [Report CE 95-03]. Los Angeles, USA: University of Southern California; 1995.
[59] Lee VW, Trifunac MD. Pseudo relative velocity spectra of strong earthquake ground motion in California [Report CE 95-04]. Los Angeles, USA: University of Southern California; 1995.
[60] Lee VW, Trifunac MD. Seismic hazard maps in Serbia. Soil Dyn Earthq Eng 2017.
[61] Lee VW, Trifunac MD. Seismic hazard maps in Macedonia. Soil Dyn Earthq Eng 2017;100:504–17.
[62] Lee VW, Trifunac MD, Todorovska MI, Novikova EI. Empirical equations describing attenuation of the peaks of strong ground motion, in terms of magnitude, distance, path effects and site conditions [Report CE 95-02]. Los Angeles, USA: University of Southern California; 1995.
[63] Lee VW, Trifunac MD, Bulajić B, Manić M. A preliminary empirical model for frequency-dependent attenuation of Fourier amplitude spectra in Serbia from the Vrancea earthquakes. Soil Dyn Earthq Eng 2016;83:167–79.
[64] Lee VW, Trifunac MD, Bulajić B, Manić M. Preliminary empirical scaling of pseudo relative velocity spectra in Serbia from the Vrancea earthquakes. Soil Dyn Earthq Eng 2017;86:41–54.
[65] Lee VW, Trifunac MD, Bulajić B, Manić M, Herak D, Herak M. Seismic microzoning of Belgrade. Soil Dyn Earthq Eng 2017;97:395–412.
[66] Lee VW, Trifunac MD, Bulajić B, Manić M, Herak D, Herak M. Seismic microzoning of Kraljevo. Izgradnja 2017;71(5–6):159–78.
[67] Lee VW, Trifunac MD, Bulajić B, Manić M, Herak D, Herak M, Dimov G. Seismic microzoning of Skopje in Macedonia. Soil Dyn Earthq Eng 2017;98:166–82.
[68] Lee VW, Trifunac MD, Bulajić B, Manić M, Herak D, Herak M, Dimov G, Gečev V. Seismic microzoning of Stip in Macedonia. Soil Dyn Earthq Eng 2017;98:54–66.
[69] Maldonado GO, Singh MP. An improved response spectrum method for calculating seismic design response. Part 2: non-classically damped structures. Erathq Eng Struct Dyn 1991;20:637–49.
[70] Naik N, Choudhury D. Deterministic seismic hazard analysis considering different seismicity levels for the state of Goa, India. Nat Hazards 2015;75:557–80.
[71] Nath SK, Thingbaijam KKS. Probabilistic seismic hazard assessment of India. Seismol Res Lett 2012;83(1):135–49.
[72] Parvez IA, Gusev AA, Panza GF, Petukhin AG. Preliminary determination of the interdependence among strong-motion amplitude, earthquake magnitude and hypocentral distance for the Himalayan region. Geophys J Int 2001;144(3):577–96.
[73] Rice SO. Mathematical analysis of random noise. Bell Syst Tech J 1944;22:282–332.
[74] Rice SO. Mathematical analysis of random noise. Bell Syst Tech J 1945;24:46–156.
[75] Richter CF. Elementary seismology. San Francisco, U.S.A: Freeman; 1958.
[76] Rosenblueth E, Elorduy J. Response of linear systems to certain transient disturbances. Proceedings of the 4th World Conference on Earthq. Eng., Chile, A-1, 185-196; 1969.
[77] Rout MM, Kamal J Das, Das R. Probabilistic seismic hazard assessment of NW and central Himalayas and the adjoining region. J Earth Syst Sci 2015;124(3):577–86.
[78] Searle SR. Linear methods. New York: Wiley; 1971. p. 532.
[79] Sharma ML. Attenuation relationship for estimation of peak ground horizontal acceleration using data from strong-motion arrays in India. Bull Seism Soc Am 1998;88(4):1063–9.
[80] Sharma ML, Douglas J, Bungum H, Kotadia J. Ground-motion prediction equations based on data from the Himalayan and Zagros regions. J Earthq Eng 2009;13(8):1191–210.
[81] Shrikhande M. Atlas of Indian strong motion records (on CD-ROM). Roorkee: Department of Earthquake Engineering, Indian Institute of Technology Roorkee; 2001.
[82] Singh MP, Chu SL. Stochastic considerations in seismic analysis of structures. Earthq Eng Struct Dyn 1976;4:295–307.
[83] Singh MP, Mehta KB. Seismic design response by an alternative SRSS rule. Earthq Eng Struct Dyn 1983;11:771–83.
[84] Singh MP, Maldonado GO. An improved response spectrum method for calculating seismic design response, Part 1: Classically damped structures. Earthq Eng Struct Dyn 1991;20:621–35.
[85] Singh RP, Aman A, Prasad YJJ. Attenuation relations for strong seismic ground motion in the Himalayan region. Pure Appl Geophys 1996;147(1):161–80.
[86] Smeby W, DerKiureghian A. Modal combination rules for multicomponent earthquake excitation. Earthq Eng Struct Dyn 1985;13:1–12.
[87] Trifunac MD. Zero baseline correction of strong-motion accelerograms. Bull Seism Soc Am 1971;61(5):1201–11.
[88] Trifunac MD. A note on correction of strong-motion accelerograms for instrument response. Bull Seism Soc Am 1972;62(1):401–9.
[89] Trifunac MD. Preliminary empirical model for scaling Fourier amplitude spectra of strong ground acceleration in terms of earthquake magnitude, source-to-station distance, and recording site conditions. Bull Seism Soc Am 1976;66(4):1343–73.
[90] Trifunac MD. Preliminary analysis of the peaks of strong earthquake ground motion - dependence of peaks on earthquake magnitude, epicentral distance, and recording site conditions. Bull Seism Soc Am 1976;66(1):189–219.
[91] Trifunac MD. Response spectra of earthquake ground motion. J Eng Mech Div ASCE 1978;104(EM5):1081–97.
[92] Trifunac MD. Influence of local soil and geologic site conditions on fourier spectrum amplitudes of recorded strong motion accelerations [Report CE 87-04]. Los Angeles, USA: University of Southern California; 1987.
[93] Trifunac MD. Dependence of Fourier spectrum amplitudes of recorded strong earthquake accelerations on magnitude, local soil conditions and on depth of sediments. Earthq Eng Struct Dyn 1989;18(7):999–1016.
[94] Trifunac MD. Empirical scaling of Fourier spectrum amplitudes of recorded strong earthquake accelerations in terms of magnitude and local soil and geologic conditions. Earthq Eng Eng Vib 1989;9(2):23–44.
[95] Trifunac MD. How to model amplification of strong earthquake ground motions by local soil and geologic site conditions. Earthq Eng Struct Dyn 1990;19(6):833–46.
[96] Trifunac MD. Long period Fourier amplitude spectra of strong motion acceleration. Soil Dyn Earthq Eng 1993;12(6):363–82.
[97] Trifunac MD. Pseudo relatice velocity spectra of earthquake ground motion at long periods. Soil Dyn Earthq Eng 1995;14:331–46.
[98] Trifunac MD. Pseudo relative velocity spectra of earthquake ground motion at high frequencies. Earthq Eng Struct Dyn 1995;24:1113–30.
[99] Trifunac MD. The nature of site response during earthquakes, Proceedings of the NATO ARW Workshop, Borovec, Bulgaria, 3–31.
[100] Trifunac MD. Site conditions and earthquake ground motion – a review. Soil Dyn Earthq Eng 2016;90:88–100.
[101] Trifunac MD, Anderson JG. Preliminary empirical models for scaling absolute acceleration spectra [Report CE 77-03]. Los Angeles, USA: University of Southern California; 1977.
[102] Trifunac MD, Anderson JG. Preliminary empirical models for scaling pseudo relative velocity spectra [Report CE 78-04]. Los Angeles, USA: University of Southern California; 1978.
[103] Trifunac MD, Anderson JG. Preliminary empirical models for scaling relative velocity spectra [Report CE 78-05]. Los Angeles, USA: University of Southern California; 1978.
[104] Trifunac MD, Brady AG. On the correlation of seismic intensity scales with the peaks of recorded strong ground motion. Bull Seism Soc Am 1975;65(1):139–62.
[105] Trifunac MD, Lee VW. Dependence of fourier amplitude spectra of strong motion acceleration on the depth of sedimentary deposits [Report CE 78-14]. Los Angeles, USA: University of Southern California; 1978.
[106] Trifunac MD, Lee VW. Dependence of pseudo relative velocity spectra of strong motion acceleration on the depth of sedimentary deposits [Report CE 79-02]. Los Angeles, USA: University of Southern California; 1979.
[107] Trifunac MD, Lee VW. Frequency dependent attenuation of strong earthquake ground motion. Soil Dyn Earthq Eng 1990;9(1):3–15.
[108] Trifunac MD, Lee VW. Frequency dependent attenuation of strong earthquake ground motion [Report CE 85-02]. Los Angeles, USA: University of Southern California; 1985.
[109] Trifunac MD, Lee VW. Preliminary empirical model for scaling fourier amplitude spectra of strong ground acceleration in terms of earthquake magnitude, source to station distance, site intensity and recording site conditions [Report CE 85-03]. Los Angeles, USA: University of Southern California; 1985.
[110] Trifunac MD, Lee VW. Preliminary empirical models for scaling pseudo relative velocity spectra of strong earthquake accelerations in terms of magnitude, distance, site intensity and recording site conditions [Report CE 85-04]. Los Angeles, USA: University of Southern California; 1985.
[111] Trifunac MD, Lee VW. Empirical models for scaling Fourier amplitude spectra of strong ground acceleration in terms of earthquake magnitude, source to station distance, site intensity and recording site conditions. Soil Dyn Earthq Eng 1989;8(3):110–25.
[112] Trifunac MD, Lee VW. Empirical models for scaling pseudo relative velocity spectra of strong earthquake accelerations in terms of magnitude, distance, site intensity and recording site conditions. Soil Dyn Earthq Eng 1989;8(3):126–44.
[113] Wilson EL, DerKiureghian A, Bayo E. A replacement for the SRSS method in seismic analysis. Earthq Eng Struct Dyn 1981;1981(9):187–92.